HHS Public Access

Author manuscript

Ocul Surf. Author manuscript; available in PMC 2017 October 01.

Published in final edited form as:

Ocul Surf. 2016 October ; 14(4): 460–483.e3. doi:10.1016/j.jtos.2016.07.001.

Multiple Natural and Experimental Inflammatory Rabbit Lacrimal Gland Phenotypes

Austin K. Mircheff, PhD[1,2], **Yanru Wang, MD, PhD**[1], **Joel E. Schechter, MD**[3], **Meng Li, MS**[4], **Warren Tong, PharmD, MS**[5], **Mayssa Attar, PhD**[5], **Murty Chengalvala, PhD**[6], **Joe Harmuth, BS**[6], and **Jeffery J. Prusakiewicz, PhD**[7]

[1]Department of Physiology & Biophysics, Keck School of Medicine, University of Southern California, Los Angeles, CA

[2]Department of Ophthalmology, Keck School of Medicine, University of Southern California, Los Angeles, CA

[3]Department of Cell & Neurobiology, Keck School of Medicine, University of Southern California, Los Angeles, CA

[4]Bioinformatics Service, Norris Medical Library, University of Southern California, Los Angeles, CA

[5]Translational Drug Metabolism, Pharmacokinetics and Immunology, Allergan Inc., Irvine, CA

[6]Immunology Services, Covance Research Products, Denver, PA

[7]Drug Metabolism, Covance Laboratories Inc., Madison, WI, USA

Abstract

Purpose—To investigate lacrimal gland (LG) immunophysiological and immune-mediated inflammatory process (IMIP) phenotype diversity.

Methods—Ex vivo matured dendritic cells (mDC) were loaded with acinar cell microparticles (M_P). Peripheral blood lymphocytes (PBL) were activated in mixed cell reactions with mDC and injected directly into autologous, unilateral LG (1° ATD-LG) of two rabbit cohorts, one naïve, one immunized with a LG lysate membrane fraction (P_i). Autoimmune IgG titers were assayed by ELISA, MCR PBL stimulation indices (SI) by [^{3}H]-thymidine incorporation. Schirmer tests without and with topical anesthetic (STT-I, STT-I_A) and rose Bengal (RB) staining tests were performed. H&E and immunohistochemically stained sections were examined. RNA yields and selected transcript abundances were measured. Immune cell number and transcript abundance data were submitted to Principal Component Analysis (PCA).

Results—Immunizing P_i dose influenced SI but not IgG titers. STT scores were decreased, and rose Bengal scores increased, by day 118 after immunization. Previous immunization exacerbated

reprint requests to Corresponding author: Austin K. Mircheff, PhD, Department of Physiology & Biophysics, Keck School of Medicine, University of Southern California, 1333 San Pablo Street, BMT B11-A, Los Angeles, CA 90033. Tel: 323-442-1242. Fax: 323-442-2283. amirchef@usc.edu.

The authors have no commercial or proprietary interest in any concept or product discussed in this article.

scores in 1° ATD-eyes and exacerbated 1° ATD-LG atrophy. IMIP were evident in 2° ATD-LG as well as 1° ATD-LG. PCA described diverse immunophysiological phenotypes in control LG and diverse IMIP phenotypes in ATD-LG. IgG titers and SI pre-adoptive transfer were significantly associated with certain post-adoptive transfer IMIP phenotype features, and certain LG IMIP features were significantly associated with RB and STT I_A scores.

Conclusions—The underlying variability of normal states may contribute to the diversity of experimental IMIP phenotypes. The ability to generate and characterize diverse phenotypes may lead to phenotype-specific diagnostic and therapeutic paradigms.

Keywords

acinar cells; autoantigens; dacryoadenitis; dendritic cells; dry eye; keratoconjunctivitis; Sjögren disease

I. INTRODUCTION

Dry eye disease, one of the most common ophthalmic morbidities, is a disorder of the physiological system that maintains the tear film as a homeostatic *milieu extérieur* for the superficial epithelial cells of the cornea and conjunctiva. A primary dysfunction in any component of the system can have consequences that ramify throughout the system. Bron et al[1] have posited four major dry eye disease phenotypes on the basis of presumed natural history: evaporative, resulting from primary Meibomian gland (**MG**) dysfunction; aqueous deficient, resulting from primary lacrimal gland (**LG**) dysfunction; primary evaporative exacerbated by secondary LG dysfunction; and primary aqueous deficient exacerbated by secondary MG dysfunction. In a retrospective study of more than 200 patients, 35% presented with MG dysfunction, 10% with LG dysfunction, 25% with both MG dysfunction and LG dysfunction, and 29% with no evidence of either MG dysfunction or LG dysfunction.[2]

LG dysfunction, underlying or contributing to 35% of cases, can result from a variety of etiologies, including: impairment of corneal sensory innervation; side effects of systemic medications; infection-associated inflammatory processes; atrophic changes; graft-versus-host processes; autoimmune processes; or noninfectious immune-mediated inflammatory processes (**IMIP**). The atrophic and fibrotic changes frequently found in LG from elderly individuals may be sequelae of IMIP that resolved earlier in life.[3] Graft-versus-host disease is associated with severe LG histopathology and dysfunction.[4] The recognized autoimmune processes include those of Mikulicz's- or IgG4-related disease and Sjögren disease. Sjögren disease is associated with severe LG dysfunction, often in a context of focal infiltrates but otherwise mild parenchymal and stromal histopathology. Two categories of Sjögren disease, primary and secondary, are recognized, and the primary disease manifests in at least 4 non-interconvertible phenotypes.[5,6] Classical IMIP diagnoses include sarcoidosis and granulomatosis with polyangiitis (Wegener's granulomatosis).[7] Notably, however, evidence of IMIP not attributable to the recognized diagnoses is seen in a large majority of *post mortem* LG.[8,9] Moreover, the histopathological presentations that have been described in *post mortem* LG are remarkably diverse,[9] implying that there may be considerably more IMIP phenotypes than current classification and diagnostic paradigms envision.

The diversity of LG autoimmune and IMIP phenotypes suggests that ocular surface disease phenotypes related to LG dysfunction may be similarly diverse. One implication is that some LG and IMIP phenotypes may be responsive to current therapeutic modalities, while others are not. Thus, historical failure to recognize the diversity of LG autoimmune and IMIP phenotypes may have contributed to the present dearth of pharmacotherapies for dry eye disease[10] by handicapping interpretation of data from clinical trials of prospective modalities. Another implication is that some LG IMIP phenotypes may not be associated LG dysfunction.

A recent study of LG from young adult female rabbits indicates that healthy LG are immunophysiologically diverse by the time animals reach sexual maturity. Characteristics of the natural diversity suggest new insights into the diversity of IMIP phenotypes that develop later in life. They also have implications for the design of animal models that might be used to study IMIP phenotype-specific mechanisms and to develop IMIP phenotype-specific therapeutic modalities. In addition to the parenchymal cells, i.e., the epithelial cells of the acini and ducts, healthy LG are populated by macrophages (Mϕ) dendritic cells (DC), IgA^+ plasmacytes, B cells of varying maturity, and T cells of various lineages. It is known that some of the immune cells cooperate with parenchymal cells to recruit dimeric IgA-expressing B cells, direct terminal differentiation of B cells to plasmacytes, and support plasmacyte survival and production of dimeric IgA for delivery to the tear fluid. The Mϕ and DC presumably surveille the glands continuously, removing apoptotic and other cell debris. They may also cooperate with LG parenchymal cells and other immune cells to maintain tolerance to autoantigens in the cellular debris, as well as autoantigens that the parenchymal cells constitutively secrete to the interstitial space.[11,12] Total numbers of T cells and bone marrow-derived cells, and overall abundances of immune response-related gene transcripts are subject to considerable intergland variability. The variability appears to stem from both systematic and stochastic phenomena. Clusters of markers and transcripts increase systematically with exposure to environmental dryness, and other clusters increase with exposure to high environmental temperature. However, immune cell numbers and transcript abundances also are subject to considerable variability in any given setting of dryness and high temperature. Analysis of that apparently stochastic variability with Pearson's test sorts the variables to multiple correlation clusters, which may map to "functional cell clusters" or "cell networks" that develop to different extents in different glands.[13]

A simple model for the trajectories of the dryness-responsive and high temperature-responsive functional clusters at constant dryness and temperature predicts that the clusters expand exponentially over time.[13] This model suggests a general working hypothesis for the natural histories of diverse IMIP phenotypes: Functional cell clusters that develop early in life expand and evolve in response to changing signals from the environment, hormonal changes, stochastic phenomena, and emergent systematic phenomena. In many cases, they eventually manifest as inflammatory infiltrates.

If the functional cell clusters that form in a LG influence the phenotypes of IMIP that evolve over time, they also may influence the phenotypes of IMIP that have been induced experimentally. Immunization with purified or partially purified LG autoantigens causes

IMIP to develop in mouse, rat, and rabbit models.[14-18] However, the possibility that the immunization-induced IMIP might manifest diverse phenotypes has not been considered. IMIP also can be adoptively transferred to rabbit LG from ex vivo systems. The ex vivo system that has been used until now employs primary cultured acinar cells as sources of autoantigens and as surrogate antigen presenting cells. As they express major histocompatibility complex class II molecules (**MHC II**), they activate autologous peripheral blood lymphocytes (**PBL**) in mixed cell reactions (**MCR**). The activated PBL adoptively transfer IMIP to the LG when reintroduced to their autologous animals, whether by injection directly into the LG,[14] subcutaneously,[15] or intravenously.[16] Adoptively transferred IMIP phenotype diversity has been generated by use of different activated PBL preparations (i.e., unfractionated, $CD4^+$ cell-enriched, and $CD4^+$ cell-depleted).[17] However, although expression of disease was variable within every study animal cohort, cellular and molecular characteristics of the variability were not addressed. The hypothesis that the underlying state of functional cluster development influences the expression of adoptively transferred IMIP phenotypes would be difficult to investigate, as the protocols for surgically removing LG from the individual study animals; isolating acinar cells; and enriching particular activated PBL preparations from each study animal are labor intensive. Accordingly, the goals of the present report are to introduce novel and more efficient protocols for adoptively transferring LG IMIP and to introduce the application of Principal Component Analysis as a tool for analyzing and describing the diversities of immunophysiological LG phenotypes and IMIP LG phenotypes.

The new experimental protocols employed an isolated acinar cell microparticulate fraction (M_P) and an isolated LG lysate membrane phase fraction (P_i) as sources of autoantigens. In one protocol, dendritic cells (mDC) were matured from bone marrow monocytes, loaded with M_P, and used as autoantigen presenting cells in MCR with PBL. Activated PBL from each study animal were injected into their autologous OD-associated LG, designated 1° ATD_N LG. (The companion glands were designated 2° ATD_N LG.) In the second protocol, P_i in Freund's adjuvant was injected into study animals to elicit systemic cellular and humoral autoimmune responses. In the third protocol, PBL were isolated from the systemically immunized animals, activated in MCR, and injected into their autologous OD LG, designated 1° ATD_{Imm} LG. (The companion glands were designated 2° ATD_{Imm} LG.) Histopathology was evaluated in H&E stained paraffin-embedded sections; numbers of T cells and bone marrow-derived cells were determined by immunohistochemistry with frozen sections; and abundances of selected transcripts were determined by real-time RT-PCR. As found in previous studies, immune cell number and transcript abundance profiles varied considerably among control LG. As predicted, immune cell number and transcript profiles varied considerably among the LG from each study group. Despite the intragroup variability, principal component analysis (**PCA**) distinguished each study group from the control LG, and it distinguished between the 1° ATD_N LG, 2° ATD_N LG, 1° ATD_N LG, and 2° ATD_N LG in 5 of 6 pairwise comparisons. PCA also generated combinatorial functional cluster models that describe the various control-, 1° ATD-, and 2° ATD-phenotypes. Notably, the most severe histopathology and atrophy appeared in 1° ATD_{Imm} LG, and PCA distinguished multiple cellular and molecular phenotypes of severe IMIP.

II. METHODS

A. Rabbits

Female New Zealand white rabbits for this study were raised in the Covance Research Products facility at Denver, PA. Protocols performed at Covance and at University of Southern California conformed to the ARVO Resolution on the Use of Animals in Ophthalmic Research and were approved by the respective institutional animal care and use committees. Sera from diseased female non-obese diabetic (**NOD**) mice were generously provided by Dr. Sarah F. Hamm-Alvarez, Department of Pharmacology & Pharmaceutical Sciences, School of Pharmacy, University of Southern California. LG were removed from control and experimental animals at necropsy and divided into portions to be placed in RNA-Later, formalin, and OCT. Figure 1 summarizes the sequences of protocols, from isolation of the autoantigen preparations, M_P and P_i, to adoptive transfer of activated PBL to their autologous naïve and systemically immunized rabbits.

B. Acinar Cells

Acinar cells were isolated as described by Guo et al[18] and maintained for 48 hr in a medium containing 50% Ham's F-12 medium and 50% Dulbecco's low glucose Modified Eagle's medium and supplemented with penicillin, streptomycin, glutamine, hydrocortisone, n-butyric acid, insulin, transferrin, sodium selenite, L-thyroxine, laminin, and carbachol, as described by Gierow et al.[19]

C. Autoantigen Preparations

1. P_i and S_i Fractions—LG were suspended in ice-cold isolation buffer containing 5% sorbitol, 5 mM histidine-imidazole buffer, pH 7.5, and 0.5 mM NaEDTA and supplemented with the protease inhibitors, aprotinin, leupeptin, PMSF, TAME, and TLCK. Over ice, glands were cut into small pieces with a pair of scalpel blades. In an ice-water bath, tissue pieces were lysed at ~30,000 rpm for 10 minutes with an Omni Tissue Homogenizer (Kennesaw, GA). Reconstituted acini were sedimented by centrifugation and resuspended in the protease inhibitor-supplemented isolation buffer. Acini were lysed by sequences of 20 passages through 21G, 25G and 27G needle. Lysates were centrifuged 1000 × g × 10 min to sediment extracellular matrix material and other debris. The resulting supernatants were centrifuged at 250,000 × g × 60 min to sediment the total membrane phase fraction (P_i). The remaining supernatant fluid (S_i) was centrifuged on Centricon® filters (EMD Millipore, Billerica, MA) to concentrate soluble proteins larger than 10 kDa.

2. M_P Fraction—Supernatant culture media were centrifuged at 1000 × g × 10 min to remove intact cells and extracellular matrix material. The resulting supernatants were centrifuged at 250,000 × g × 60 min to sediment the microparticulate phase fraction (M_P).

D. Protein Determination

Protein concentrations in the various fractions were determined with the Bradford assay (Bio-Rad, Richmond, CA). Bovine serum albumin was used as standard.

E. Systemic Immunization

1. Immunization—Protocols for immunization, collection of test bleeds, and initial ocular surface status evaluations were performed in the Covance facility at Denver, PA. The P_i fraction was used to systemically immunize rabbits. Dual immunization doses, each containing 0.25, 1.0, 2.5, or 10 mg protein emulsified in complete Freund's adjuvant, were administered to pairs of rabbits, one dose intramuscularly, the other dose subcutaneously. Booster doses containing the same respective amounts of protein in Freund's incomplete adjuvant were administered subcutaneously on day 21. A final booster dose containing 10 mg protein in Freund's incomplete adjuvant was administered to each animal subcutaneously on day 87. Blood was drawn and serum obtained on days 0, 31, 87, and 118. On day 180, the animals were transferred to the University of Southern California Health Sciences Campus Vivarium.

2. ELISA—Acinar cells were isolated and maintained in primary culture for 2 days, as catabolism during this culture period reduces background IgG content. The cells were lysed and the P_i fraction was isolated and coated onto ELISA plates (Greiner, 96-well, polystyrene, flat-bottom, high binding, product #655061). After incubation with serial dilutions of sera from each of the test bleeds, plates were washed to remove unbound proteins. Captured immunoglobulin was detected with horseradish peroxidase-conjugated donkey anti-rabbit IgG (Jackson ImmunoResearch) at 1:5,000 in assay diluent (cat# 711-035-152, lot# 107844). The enzyme Q7 activity retained on the plate was measured using ABTS peroxidase substrate (1-component) from KPL, prod# 50-66-01, lot# 121019). ELISA assay results are reported as 50% titers (reciprocal of dilution at which 50% of maximum absorbance was observed).

3. Western Blotting—P_i, S_i, and M_P were isolated from acinar cells and suspended in loading buffer containing SDS and dithiothreitol and denatured in boiling water for 5 min. Aliquots containing 30 mg protein were resolved by electrophoresis on 15% polyacrylamide gels. Proteins were then transferred to Immobilon-FL® membranes (EMD Millipore). Strips representing lanes with replicate M_P samples were cut and probed with sera from diseased female NOD mice or from each of the immunized rabbits. After washing, the strips were probed with goat anti-mouse IgG or goat anti-rabbit IgG labeled with infrared fluorescent dye 800. Images were captured with an Odyssey® Scanning Infrared Fluorescent Imaging System (Li-Cor, Lincoln, NB).

F. Ex Vivo Maturation, Loading, and Activation of Dendritic Cells (mDC)

Bone marrow was collected from femurs of from 1 to 3 rabbits per experiment. The methods described by Cody et al[20] were used to isolate monocytes. After treatment with RBC Lysis Buffer (BioLegend) and washing, dispersed bone marrow cells were suspended in complete medium (RPMI 1640 medium supplemented with L-glutamate, 10% fetal bovine serum, 25 mM HEPES, and 2% penicillin-streptomycin) and plated at 2-4 × 10^6 cells/mL. Nonadherent cells were removed, and adherent monocytes were washed with RPMI 1640 and incubated in complete medium. Recombinant human GM-CSF (800 U/mL) and IL-4 (500 U/mL) were added on culture days 1, 3, day 5. M_P (10 μg protein/mL) was added to the maturing DC at on culture day 6. They were then activated by addition of LPS (10 μg/mL)

on culture day 7. They were washed and resuspended in complete medium at a concentration of 12×10^5 cells/mL on culture day 8, and dispensed to wells of 96-well plates in 100 μL aliquots and to wells of 24-well plates in aliquots of 500 μL. They were then gamma-irradiated at 2500~3000 RAD.

G. Ex Vivo Mixed Cell Reactions

Protocols for MCR were similar to those described by Q2 Guo et al[21] and de Saint Jean et al.[11] On monocyte culture day 8, PBL were obtained by centrifugation on Ficoll-Paque,® washed 3 times by centrifugation in Hank's balanced salt solution, and resuspended in complete medium to a concentration of 1×10^6 cells/mL. PBL were added to wells containing irradiated mDC in a 10:1 ratio. [^{3}H]-thymidine was added to 96 well plates on day 11, and on day 12 activated PBL were harvested for liquid scintillation counting to assess proliferation. SI were calculated as (mean [^{3}H] incorporation in MCR)/(mean [^{3}H] incorporation by PBL alone). PBL from 24-well plates were washed, and resuspended in RPMI at a concentration of 5×10^6 cells/mL for adoptive transfer.

H. Adoptive Transfer by Injection of Activated PBL

Methods for adoptive transfer of activated PBL from ex vivo MCR back to LG of their autologous rabbits were as described by Guo et al[22] and Zhu et al.[19] Rabbits were anesthetized with intramuscular injections of 100 mg/kg ketamine-xylazine. The inferior lobe of the OD LG was exposed with a conjunctival incision and blunt dissection of the fascia. A Stepper pipette was used to inject 10 μL aliquots of activated PBL at 20 points dispersed about the exposed portion of the gland. The incision was rinsed with sterile Hank's solution containing neomycin and sutured with Vicryl® 6.0 (Ethicon Inc, Cincinnati, OH).

I. Ocular Surface Assessments

Ocular surface status was assessed at the Covance Denver, PA, facility with the fluorescein staining test and Schirmer Tear Test without anesthesia (STT-I) on day 1, day 31, day 87, and day 118. Ocular surface status was assessed in the USC Vivarium with STT-I, STT-I after instillation of 1 drop ophthalmic proparacaine (STT-I_A), and the rose Bengal staining test on day 185, day 213, day 227, and day 255. Methods for STT-I and rose Bengal staining were as described by Zhu et al.[19]

J. Tissue Collection

At necropsy, each LG was divided into 3 equal portions, which were placed in formalin for paraffin embedding and H&E staining, OCT for immunohistochemistry, and RNALater® for RNA extraction.

K. Real-Time RT-PCR

Methods for mRNA extraction, reverse transcription, and real-time polymerase chain reaction (PCR) were as described by Thomas et al.[21]

L. Immunohistochemistry and Image Analysis

OCT embedded tissues were cut at ~8-10 μm, fixed with paraformaldehyde/zinc; blocked with Aurion® blocking solution containing normal donkey serum; and incubated either with goat anti-rabbit RTLA (Rabbit T Lymphocyte Antigen, Cedarlane Labs, Burlington, NC) as a marker for T cells or with mouse anti-rabbit CD18 (Antigenix America, Huntington Station, NY) as a marker for bone marrow-derived cells. Biotin-SP-conjugated donkey-anti-goat IgG, donkey anti-mouse IgG, and peroxidase-conjugated streptavidin were from Jackson ImmunoResearch Laboratories (West Grove, PA). 3,3′diaminobenzide was from Sigma-Aldrich (St. Louis, MO). Sections were counterstained with Hematoxylin QS® (Vector Laboratories, Burlingame, CA). The percentages of total cells immunopositive for RTLA and CD18 were determined with MetaMorph® Microscopy Automation and Image Analysis Software.

M. Data Analysis

ANOVA, linear regression, and nonlinear regression analyses were done with SigmaPlot 13® (Systat Software, Chicago, IL). Principal component analyses were done with the Partek Genomics Suite® (Partek Inc., St. Louis, MO).

III. RESULTS

A. Autoantigen Preparations

Circulating immune complexes from patients with Sjögren syndrome and other autoimmune diseases contain multiple disease specific autoantigens.[23] Several of the autoantigens labeled by autoantibodies in sera from patients with primary Sjögren syndrome appear to be preferentially associated with the membrane phase of lacrimal gland lysates.[24] IgG in tear fluid from normal subjects and from patients with LG dysfunction and diagnoses other than Sjögren syndrome have been reported to recognize distinct spectra of bands[25] in Western blots a bovine retina lysate soluble phase fraction[26]; potential autoantigens in corresponding membrane phase fraction were not addressed. As acinar cells constitutively secrete exosomes (M_P) to their underlying interstitial space, M_P may represent the predominant autoantigen signature perceived by immune system. Serum IgG from diseased female NOD mice was used to label potential cross-reactive autoantigens in Western blots of the rabbit acinar cell lysate fractions, P_i and S_i, and the secreted microparticle fraction, M_P. As shown in Figure 2, some labeled bands were relatively enriched in P_i, which represents the total post-nuclear membrane phase. Other labeled bands were relatively enriched in S_i, which represents the total soluble phase. Bands corresponding to both the labeled P_i bands and the labeled S_i bands were highly enriched in M_P. Accordingly, M_P were used as sources of acinar cell autoantigens for activating PBL in *ex vivo* MCR. P_i, which can be readily obtained in large quantities from lacrimal gland lysates, was used as the immunogen for to systemic immunization.

B. Ex Vivo Mixed Cell Reactions

To confirm that dendritic cells (mDC) loaded with M_P are capable of activating allogeneic PBL and to survey the variability of responses, monocytes were obtained from femurs of 3

rabbits, matured to mDC (mDC.01, mDC.02, mDC.03), loaded with M_P, stimulated with LPS, and placed in MCR with PBL from each of 3 additional rabbits (PBL.04, PBL.05, PBL.06). As shown in Figure 3, PBL proliferated in 8 of the 9 MCR, with [^{3}H]-thymidine incorporation rates ranging from 2.6-fold to 89.7-fold higher than the rates of PBL cultured in the absence of mDC. (The ratio of [^{3}H]-thymidine incorporation rates in the presence and absence of mDC is referred to as the stimulation index, or SI.) PBL.05 consistently proliferated at the lowest rates. In 2 MCR of 3, PBL.06 proliferated at the highest rate, and in 1 MCR of 3, PBL.04 proliferated at the highest rate. These findings indicate that variability across the PBL preparations and variability across the mDC preparations contributed to the variability of the proliferation rates. As mDC.03 consistently stimulated intermediate rates of PBL proliferation, the PBL that had been activated by mDC.03 were used for the Protocol 1 adoptive transfer experiment (Section III.D.1).

C. Systemic Immunization

It was predicted that immunizing animals with P_i cause ocular surface disease and exacerbate the severity of the adoptively transferred LG IMIP.

1. Humoral Autoimmune Responses—The magnitudes and time-courses of the humoral autoimmune responses to immunization with P_i varied considerably across the 8 animals that were immunized. As shown in Figure 4A, the IgG titers in 2 animals were relatively high after the initial immunization and first booster injection; they continued to increase until the second booster injection; and they decreased after second booster injection. The titers in 2 animals remained relatively low after the first boost; they reached moderately high levels by the time of the second boost; and they decreased after the second boost. The titers in 3 animals were low-to-moderate by the time of the first boost; they decreased by the time of the second boost and remained low after the second boost. The titer in 1 animal (#492) changed negligibly over the entire time-course. By the final draw on day 118, the titers were from 1.14 to 7.3 fold higher than baseline. Overall Western blot signal intensities for IgG from the animals with the 5 highest titers increased in the sequence #485 < #487 ~ #489 < #491 < #488 (Figure 4B). This sequence was similar, but not identical, to the sequence of increasing titers (#485 < #487 ~ #489 < #488 < #491). The differences for #488 and #491 may have reflected differing accessibilities of determinants in non-denatured P_i, used in the ELISA, and denatured P_i, used in the Western blots, such that IgG from rabbit #488 preferentially recognized determinants in denatured P_i, while IgG from rabbit #491 preferentially recognized non-denatured determinants. Neither the IgG titers nor the overall Western blot signal intensities correlated significantly with the initial immunizing P_i protein doses (Figure 4C). For example, of the 2 animals that had received the highest initial P_i protein dose, #491 generated the highest titer and #492 generated the lowest. Taken together, these findings indicate that intrinsic immunophysiological differences between the animals played large roles in determining the time-courses and magnitudes of the humoral autoimmune responses.

2. Cellular Autoimmune Responses—MCR SI of PBL from the systemically immunized animals were used to assess the cellular autoimmune responses after immunization with P_i. Figure 3 shows that intrinsic phenomena influenced SI of PBL from

naïve animals. Intrinsic phenomena also influenced the cellular autoimmune responses, as SI differed between animals that received the same dose of P_i (Figure 4D). Despite the intrinsic sources of variability, linear regression analysis detected a significant association between increasing PBL SI and increasing initial immunizing P_i protein doses (R^2 = .693, P=.0064).

D. Ocular Surface Manifestations after Adoptive Transfer and after Systemic Immunization

1. Protocol 1—Time-courses of SST-I, STT-I_A, and rose Bengal staining scores after activated PBL preparations PBL.04, PBL.05, and PBL.05 from naïve animals (Figure 3) were injected into their autologous, OD LG are shown in Figures 5A, 5B, and 5C. The mean SST-I and STT-I_A scores in the 1° ATD_N eyes decreased by day 7 and remained low at day 35. The mean rose Bengal staining scores in the 1° ATD_N eyes increased by day 7 (P=.018) and remained elevated at day 37 (P=.024). STT-I scores in the 2° ATD_N eyes decreased slightly but significantly by day 7, then appeared to rebound by day 35. STT-I_A scores in the 2° ATD_N eyes did not differ significantly from baseline scores. The mean rose Bengal staining scores in the 2° ATD_N eyes tended to increase, but differences from the mean baseline score were not statistically significant.

2. Protocol 2—Time-courses of SST-I, STT-I_A, and rose Bengal staining scores after rabbits #485-#492 were immunized with P_i are shown in Figures 5D, 5E, and 5F. Comparisons with Figures 5A, 5B, and 5C demonstrate that ocular surface disease developed after rabbits were systemically immunized and that adoptive transfer of disease to LG exacerbated surface disease manifestations in the 1° ATD_{Imm} eyes. The mean STT-I score increased modestly (by 26%) but significantly (P=.030) by day 87, i.e., after the initial immunization and first booster injection (Figure 5D). However, the mean scores obscure a systematic variation across the individual animals. The STT-I scores on day 87 were increased more substantially (by 55% to 106%) and consistently in the 2 animals that had generated the weakest humoral autoimmune responses (Figure 5G), and the scores could be described as having decreased with increasing IgG titers according to an exponential decay relationship (R^2 = .435, P=.0245). The increases of STT-I scores in the low IgG titer animals were reversed after the second booster injection, such that the mean STT-I score was slightly but significantly lower than the baseline value (P<.001) by day 185. The transient STT-I score increases are of interest, however, as they suggest that low IgG titers were associated with ocular surface- or LG IMIP phenotypes that increased tear fluid production.

STT-I_A and rose Bengal staining tests were not performed on the cohort of systemically immunized animals until after they were transferred to the USC Vivarium. However, comparison with the baselines values for the cohort of naïve animals indicates that the mean STT-I_A score decreased below the baseline value (Figure 5E), and the mean rose Bengal staining score increased above the baseline value (Figure 5F), by day 185 after systemic immunization. As was noted in Figure 4C, immunized animal PBL SI were related to the initial immunizing P_i doses. As shown in Figure 5H and Figure 5I, day 185 rose Bengal staining scores also were significantly related to the initial P_i doses (P=.0101, R^2 = .387) as well as to the PBL SI (P=.0065, R^2 = .421), which were determined on day 199.

3. Protocol 3—By 2 weeks after adoptive transfer, STT-I scores and STT-I_A scores decreased (Figure 5D and Figure 5E), and rose Bengal staining scores increased (Figure 5F) in the 1° ATD_{Imm} eyes. Adoptive transfer appeared not to influence STT-I scores or rose Bengal staining scores in the 2° ATD_{Imm} eyes. However, the mean STT-I_A score in the 2° ATD_{Imm} eyes increased significantly (P=.030), reaching the baseline value by day 255 after systemic immunization. As the mean STT-I_A score appears to have been increasing linearly with time (R^2 = .9996, P=.011), it is possible that it would have increased further if the animals had been followed longer. As rose Bengal staining scores remained elevated in the 2° ATD_{Imm} eyes on day 255, and IMIP 3 were detected in the 2° ATD_{Imm} LG (Section E and Section F) taken at necropsy on day 256, the increasing mean 2° ATD_{Imm} STT-I_A score suggests that IMIP phenotypes associated with increased tear fluid production were continuing to evolve.

E. Histopathology and Immune Cell Infiltration after Adoptive Transfer and after Systemic Immunization and Adoptive Transfer

1. Atrophy: Protocol 1 and Protocol 3—mRNA yields were used as indirect measures of the amount of tissue surviving in the individual glands. The highest, mean, and lowest mRNA yields from control LG are illustrated in (Figure 6). Yields from all of the 1° ATD_N, 2° ATD_N, 1° ATD_{Imm}, and 2° ATD_{Imm} LG also are shown. Both the 1° ATD_N LG and the 2° ATD_N LG appeared to have undergone similar, moderate degrees of atrophy. In accord with the hypothesis that prior systemic immunization would promote development of more severe adoptively transferred LG IMIP phenotypes, atrophy in the 1° ATD_{Imm} LG ranged from moderate, in 1° ATD_{Imm} LG.490, to extremely severe, in 1° ATD_{Imm} LG.488 and 1° ATD_{Imm} LG.485. mRNA yields in 5 of the 2° ATD_{Imm} LG were within the range of control values. However, 2° ATD_{Imm} LG.492 and 2° ATD_{Imm} LG.488 were moderately atrophied, and 2° ATD_{Imm} LG.491 was severely atrophied.

2. Histopathology

a. Protocol 1: 1° ATD_N LG.04 presented with areas of moderate lymphocytic infiltration and extensive fibrosis (Figure 7A), and also with areas of extensive lymphocytic infiltration and moderate fibrosis (Figure 7B). The histopathological presentations of 1° ATD_N LG.05 and 1° ATD_N LG.06 resembled the more heavily infiltrated, less fibrotic regions of 1° ATD_N LG.04 depicted in Figure 7B. The 2° ATD_N LG from the naive animals (not shown) presented with less fibrosis and less infiltration than 1° ATD_N LG.05 and 1° ATD_N LG.06.

b. Protocol 3: The 1° ATD_{Imm} LG from the systemically immunized animals presented diverse histopathological patterns suggesting multiple IMID phenotypes. 1° ATD_{Imm} LG. 485 (Figure 7D) and 1° ATD_{Imm} LG.486 (Figure 7E) presented with more severe parenchymal disruption and more fibrosis. 1° ATD_{Imm} LG.488 (Figure 7C) and 1° ATD_{Imm} LG.491 (Figure 7F) presented with less severe parenchymal disruption and less fibrosis. As shown in Figure 6, 1° ATD_{Imm} LG.485 and 1° ATD_{Imm} LG.488 underwent very severe atrophy. 1° ATD_{Imm} LG.486 and 1° ATD_{Imm} LG.491 underwent somewhat less severe atrophy, with 1° ATD_{Imm} LG.491 affected more than 1° ATD_{Imm} LG.486. On this qualitative basis, the 4 glands would appear to manifest 4 different IMIP phenotypes. As will be shown in Section III.H.1, differences between the cellular and molecular phenotypes 1°

ATD_{Imm} LG.486 and 1° ATD_{Imm} LG.491 may account for the marked differences between their histopathological presentation.

3. Infiltration by Bone Marrow-Derived Cells and T Cells: Protocol 1 and Protocol 3—The quantitative findings after immunohistochemical staining for CD18, generally expressed by bone marrow-derived cells, and RTLA, expressed by rabbit T lymphocytes, are presented in Figure 8. In the naïve rabbits, the mean percentage of $CD18^+$ cells increased significantly in both the 1° ATD_N LG and the 2° ATD_N LG, while the mean percentage of $RTLA^+$ cells increased significantly only in the 1° ATD_N LG. In the systemically immunized animals, the $CD18^+$ cell percentage and the $RTLA^+$ cell percentage increased significantly in both the 1° ATD_{Imm} LG and the 2° ATD_{Imm} LG. These findings confirm that IMIP were ongoing in 2° ATD_N LG and 2° ATD_{Imm} LG associated with eyes that had normal (Figure 4A and Figure 4D) or near-normal (Figure 4B and Figure 4E) STT-I and $STT\text{-}I_A$ scores.

F. Immune Response-Related Gene Transcript Expression, Protocol 1 and Protocol 3

Mean transcript abundances in the Control LG and ATD LG are presented in Figure 9. (1° ATD_{Imm} LG.485 and 1° ATD_{Imm} LG.488 (Figure 5) had atrophied so severely that transcript abundances could not be measured by real-time RT-PCR). The mean abundances of mRNAs for IL-4, CD4, CCR5, CXCL8, BAFF, IL-18, IL-1β, CTLA-4, IL-1α, IL-12A, and CCL28 were significantly increased in 1° ATD LG from both cohorts of animals. The mean abundances of mRNAs for CCL4, CCL21, CXCL13, CD28, CCL2, CD8, and MMP-9 were significantly increased in the 1° ATD_N LG. The mean abundances of mRNAs for perforin, IL-18R, and IL-6 were significantly increased in the 1° ATD_{Imm} LG. The mean abundances of mRNAs for MMP-9 and CD1d were significantly higher in the 1° ATD_N LG than in the 1° ATD_{Imm} LG. The mean abundances of IL-4 mRNA were significantly increased in both the 2° ATD_N LG and the 2° ATD_{Imm} LG. The mean abundances of mRNAs for CD4 and CCR5 were significantly increased in the 2° ATD_N LG. The mean abundance of CXCL8 mRNA was significantly increased, and the mean abundance of CD1d mRNA was significantly decreased, in the 2° ATD_{Imm} LG. There were trends toward increasing mean abundances of other transcripts in the 1° ATD LG and 2° ATD LG from both cohorts of animals and trends toward differences in the mean abundances of other transcripts between the 1° ATD_N LG and the 1° ATD_{Imm} LG, and between the 2° ATD_N LG and the 2° ATD_{Imm} LG. These trends were not statistically significant, but it appears that they were biologically significant, as wide variations about the mean values reflected the diversities of the IMIP phenotypes that developed in each of the 4 groups of LG.

G. Principal Component Analysis

Principal Component Analysis was used obtain simplified depictions of the multidimensional differences between control LG, 1° ATD_N LG, 2° ATD_N LG, 1° ATD_{Imm} LG, and 2° ATD_{Imm} LG. Principal components are the independent sources of variation that can be isolated from measurements of multiple variables in multiples samples.[27] The analysis can generate as many as n_v-1 principal components when n_v, the number of variables, is greater than the number of samples. In the context of gene expression analyses, principal components have been referred to as “latent variables,” “latent causes,”

"pathways," "metagenes," and "supergenes."[28,29] PCA has been used both to describe associations between multiple genes and defined disease phenotypes,[30,31] and also to describe phenotypes in terms of empirically determined gene expression associations.[32]

1. Principal Component Projections, Control LG, 1° ATD_N LG, 2° ATD_N LG, 1° ATD_{Imm} LG, and 2° ATD_{Imm} LG—Figure 10 illustrates the projections of the control LG, 1° ATD_N LG, 2° ATD_N LG, 1° ATD_{Imm} LG, and 2° ATD_{Imm} LG with respect to the first three principal components determined by analysis of the pooled data from the 5 groups of glands. As summarized in the insert to Figure 10, the mean projections of the 1° ATD_N LG and 1° ATD_{Imm} LG differed from the control LG mean projections with respect to both PC 1 and PC 2. The 2° ATD_N LG differed from the control LG with respect to PC 1. The 2° ATD_{Imm} LG differed from the control LG with respect to PC 2. Five of the 6 remaining comparisons also were significant with respect to PC 2 or with respect to both PC 1 and PC 2. The one mean projection comparison that was not significant with respect to either PC 1 or PC 2 was between the 1° ATD_N LG (n = 3) and the 2° ATD_N LG (n = 3). Notably, the PC 1 projections of the control glands spanned a larger range of values than did the projections of any of the groups of ATD LG, illustrating the high degree of underlying natural immunophysiological diversity.

2. Functional Clusters, Control LG, 1° ATD_{Imm} LG, and 2° ATD_{Imm} LG—The concept that clusters of cells functioning coordinately in the LG emerged from observations that Pearson's test sorted mRNA abundances and immune cell numbers into multiple correlation clusters and that clusters of mRNAs responded similarly to increasing degrees of environmental dryness and increasingly high temperatures. In isolating principal components, PCA determines the contribution ("loading") each variable makes to each principal component. Thus, PCA identifies instances in which the same variable contributes to multiple principal components. For the purposes of this study, the set of variables that contributed loadings of the same sign to a principal component was modelled as mapping to a functional cell cluster. Almost all of the principal components identified received both positive and negative loadings; in these cases, the two sets of variables that contributed loadings of opposite signs to the same principal component were modelled as mapping to a dyad of functional clusters that behaved reciprocally. Taken together, a gland's set of projections in the principal component space and the sets of variables that contribute strong loadings to the principal components represent a combinatorial model of the gland's phenotype.

The hypothesis that the functional clusters that formed in the 1° ATD_{Imm} LG and the 2° ATD_{Imm} LG differed from each other and from the control LG functional clusters was tested by submitting the data from each of the 3 groups of glands to separate principal component analyses. Results for the first 3 principal components for each group are presented in Figure 11, Figure 12, and Figure 13. Included in each are a 3-dimensional plot and a table of LG projections; lists of the variables that contributed loadings ≥0.300, designated $\{^{I}PC\ J^{\oplus}\}$ and the variables that contributed loadings ≤−0.300, designated $\{^{I}PC\ J^{\ominus}\}$, arranged according to cell types in which they typically are expressed; and immune cell number and transcript abundance profiles of individual glands. To facilitate comparisons, Table 1 presents the $\{^{I}PC$

$1^{\oplus}$} and {^{I}PC $1^{\ominus}$} transcript sets for the 3 groups of LG. Table 1 also presents variable sets {$^{V(82\%29°)}$PC $1^{\oplus}$} and {$^{V(82\%29°)}$PC $1^{\ominus}$}, which were identified by PCA of data from a group of LG that were described previously and analyzed with Pearson's test.[13]

a. Control LG: Variable set {^{Cont}PC $1^{\ominus}$} includes 18 of the 22 variables that PCA assigned to {$^{V(82\%29°)}$PC $1^{\ominus}$} (Table 1); the 82% overlap suggests that the variable sets map to two homologous functional clusters. The homology illustrates the robustness of a core functional cluster that develops adaptively, in response to signals related to dryness, and reactively, in response to signals from other functional clusters.[13] {^{Cont}PC $1^{\ominus}$} differs from {$^{V(82\%29°)}$PC $1^{\ominus}$} in that it lacks mRNAs for IL-1β, PRL, CCL21, and CCL28 and in that it additionally includes mRNAs for TNF-α, MHC I, and CXCL8; (perforin mRNA was not assayed in the earlier study). The differences may be related to differences between the environmental conditions the 2 groups of animals experienced.

The composition of variable set {^{Cont}PC $1^{\ominus}$} (Figure 11) suggests a functional cluster model that includes acinar epithelial cells expressing CCL2 mRNA; ductal epithelial cells expressing CCL4 mRNA; Mϕ possibly of several phenotypes, collectively expressing mRNAs for IL-1α, IL-6, TNF-α; DC possibly of several phenotypes, collectively expressing mRNAs for MHC I, MHC II, CD1d, CXCL13, BAFF; and T cells, possibly of several lineages, collectively expressing mRNAs for RTLA, CD4, CD8, CTLA-4, CD28, IL-10, IL-17A, and perforin. {^{Cont}PC $1^{\ominus}$} also includes mRNA for CXCL8, which may be expressed by many different cell types, and mRNA for the CCL4 receptor, CCR5, which is expressed by T cells and certain B cells. The reciprocal variable set, {^{Cont}PC $1^{\oplus}$}, suggests a functional cluster model that includes Mϕ expressing CD18 and mRNA for IL-18.

Variable set {^{Cont}PC $2^{\ominus}$} suggests a functional cluster model that includes Mϕ expressing mRNA for MMP-9; T cells, possibly of several lineages, collectively expressing RTLA and mRNAs for CTLA-4, CD28, and IL-18R; and DC expressing mRNA for CXCL13. The reciprocal variable set, {^{Cont}PC $2^{\oplus}$}, suggests a functional cluster model that includes acinar cells expressing PRL; Mϕ expressing mRNA for IL-6; T cells, possibly of several lineages, expressing mRNAs for CD4, IL-10, IL-12A, and perforin; and cells, possibly of multiple types, expressing mRNA for CXCL8.

Variable set {^{Cont}PC $3^{\ominus}$} suggests a functional cluster model that includes acinar epithelial cells expressing mRNA for CCL2; Mϕ expressing mRNAs for IL-18 and MMP-9; and T cells expressing mRNAs for CD8 and IL-12A. The reciprocal variable set, {^{Cont}PC$3^{\oplus}$}, suggests a functional cluster model that includes Mϕ expressing CD18; T cells expressing mRNA for IL-18R; and DC expressing mRNA for MHC I.

b. 1° ATD_{Imm} LG: Variable set {$^{1°\ ATD(Imm)}$PC $1^{\oplus}$} (Table 1 and Figure 12) includes 13 of the 20 variables represented in {^{Cont}PC $1^{\ominus}$}. It differs from variable set {^{Cont}PC $1^{\ominus}$} in that it additionally includes $CD18^{+}$ cells; mRNA for CCL21, classically expressed by stromal reticular fibroblasts; and mRNAs for IL-1β, IL-18, and MMP-9. It also differs from {^{Cont}PC $1^{\ominus}$} in that it does not include mRNAs for CD4, IL-10, IL-17A, CD1d, perforin, or MHC II. Notably, mRNAs for CD4, IL-10, IL-17A, perforin, CD1d are instead included in the

reciprocal variable set, {$^{1°\ ATD(Imm)}$PC $1^{\ominus}$}, and {$^{1°\ ATD(Imm)}$PC $1^{\ominus}$} additionally includes mRNAs for PRL and IL-12A.

c. 2° ATD_{Imm} LG: Variable set {$^{2°\ ATD(Imm)}$PC $1^{\ominus}$} (Table 1 and Figure 13) includes 11 of the 18 (61%) variables that are included in {$^{1°\ ATD(Imm)}$PC $1^{\oplus}$}: mRNAs for CCL2 and CCL4; $RTLA^{+}$ cells and mRNA for CD8; $CD18^{+}$ cells and mRNAs for IL-1β, IL-6, and IL-18; mRNAs for MHC I and CXCL13; and mRNA for CCR5. However, it differs in that it additionally includes mRNAs for CD4, IL-18R, and MHC II. It also differs in that it does not include mRNAs for BAFF, CCL21, CD28, CTLA-4, IL-1α, MMP-9, and TNF-α. The reciprocal variable set, {$^{2°\ ATD(Imm)}$PC $1^{\oplus}$}, resembles variable set {$^{1°\ ATD(Imm)}$PC $1^{\oplus}$} in that it includes mRNAs for IL-10, IL-12A, and perforin, but differs in that it also includes mRNA for CCL28 and in that it does not include mRNAs for CD4 and IL-17A.

H. Functional Clusters and Mediators Associated with LG Atrophy, Ocular Surface Inflammation, and Altered Tear Fluid Production

Figure 5G shows that increased STT-I scores prior to the high dose booster immunization were associated with lower IgG titers, and Figure 5H shows that increased rose Bengal staining scores prior to adoptive transfer were associated with more robust cellular autoimmune responses. Evidence also links features of ocular surface pathology, LG histopathology, and tear fluid production with specific LG functional clusters and mediators after adoptive transfer.

1. LG Atrophy—Among the 1° ATD_{Imm} LG in which transcript abundances could be measured, RNA yield could be described as a linear function of the $^{1°\ ATD(Imm)}$PC 1 projections and the $^{1°\ ATD(Imm)}$PC 2 projections according to Equation 1.

$$^{1°ATD(Imm)}LG \quad RNA = 0.117 + \left(0.0194 \cdot {}^{1°ATD(Imm)}PC1\right) - \left(0.0299 \cdot {}^{1°ATD(Imm)}PC2\right)$$

$$R^2 = 0.948, \quad P = .0120 \qquad (1)$$

Thus, increasing LG atrophy was associated with increasingly negative $^{1°\ ATD}$PC 1 projections and with increasingly positive $^{1°\ ATD}$PC 2 projections. As mRNAs for IL-17A and for perforin, a mediator associated with antibody-dependent cell-mediated cytolysis, are the only assayed transcripts that are included in both {$^{1°\ ATD(Imm)}$PC $1^{\ominus}$} and {$^{1°\ ATD(Imm)}$PC $2^{\oplus}$} (Figure 12), it would be straightforward to suggest that perforin played a direct role, and IL-17A an indirect role, in LG atrophy.

Comparing 1° ATD_{Imm} LG.486 and 1° ATD_{Imm} LG.491 depicted in Figure 6, Figure 7, and Figure 12, 1° ATD_{Imm} LG.486 underwent somewhat less severe atrophy, evidently driven primarily by {$^{1°\ ATD(Imm)}$PC $1^{\ominus}$}, but it presented with more fibrosis, more parenchymal disruption and less infiltration; 1° ATD_{Imm} LG.491 underwent somewhat more severe atrophy, evidently driven primarily by {$^{1°\ ATD(Imm)}$PC $2^{\oplus}$}, but it presented with less

fibrosis, less parenchymal disruption, and more lymphocytic infiltration. As {$^{1°\ \mathrm{ATD(Imm)}}$PC $1^{\ominus}$} included mRNAs for CD4, IL-10, IL-12A, CD1d, and PRL, while {$^{1°\ \mathrm{ATD(Imm)}}$PC $2^{\oplus}$} included mRNAs for CD8, IL-18R, IL-6, and MHC I, differences between the functional clusters to which the variable sets match may account for the different histopathological patterns.

Among the 2° $\mathrm{ATD_{Imm}}$ LG, RNA yield could be described as a linear function of the abundances of mRNAs for IL-18 and MMP-9 according to Equation 2.

$$^{2°\,ATD(Imm)}LG \quad RNA = 1.466 - \left(137.2 \cdot {}^{2°\,ATD(Imm)}IL{-}18 \quad mRNA\right) + \left(159.0 \cdot {}^{2°\,ATD(Imm)}MMP{-}9 \quad mRNA\right)$$
$$\mathrm{R}^2 = \ 0.851, \quad P = .099 \tag{2}$$

This relationship suggests that, directly or indirectly, increasing expression of IL-18 in the 2° $\mathrm{ATD_{Imm}}$ LG was associated with increasing atrophy and increasing expression of MMP-9 was associated with protection from atrophy.

2. Ocular Surface Inflammation—Figure 5H shows that increasing rose Bengal staining scores after immunization and before adoptive transfer were significantly associated with increasingly robust cellular autoimmune responses. After adoptive transfer, increasing rose Bengal scores in 1° $\mathrm{ATD_{Imm}}$ eyes were associated with increasing abundance of CD8 mRNA in 1° $\mathrm{ATD_{Imm}}$ LG (Figure 14A). This finding suggests that the severities of IMIP phenotypes in the ocular surface tissues might be related to specific mediators common to the functional clusters that express CD8 mRNA, i.e., the clusters associated with variable sets {$^{1°\ \mathrm{ATD(Imm)}}$PC $1^{\oplus}$}, {$^{1°\ \mathrm{ATD(Imm)}}$PC $2^{\oplus}$}, {$^{1°\ \mathrm{ATD(Imm)}}$PC $4^{\ominus}$}, and {$^{1°\ \mathrm{ATD(Imm)}}$PC $5^{\ominus}$} (Figure 12, Supplemental Table 2).

3. Altered Tear Fluid Production—Interestingly, neither STT-I scores nor $\mathrm{STT\text{-}I_A}$ scores were significantly associated with glandular atrophy. Evidently, other tissues contributed to tear fluid production, at least in the cases where LG functional capacity was severely compromised. This inference is consistent with previous reports that STT I scores quickly returned to their baseline values after main LG had been surgically removed in a rabbit model[19] and that STT I and STT II scores rebounded after LG had been surgically removed in a squirrel monkey model.[33] Nonetheless, decreasing $\mathrm{STT\text{-}I_A}$ scores in 1° $\mathrm{ATD_{Imm}}$ eyes were associated with increasing abundance of IL-6 mRNA in 1° $\mathrm{ATD_{Imm}}$ LG (Figure 14B). As an ex vivo study showed that exposure to IL-6 decreases the secretory $\mathrm{Cl^-}$ ion fluxes which underlie LG fluid production,[34] this association might suggest that {$^{1°\ \mathrm{ATD(Imm)}}$PC $1^{\oplus}$}, {$^{1°\ \mathrm{ATD(Imm)}}$PC $2^{\oplus}$}, and {$^{1°\ \mathrm{ATD(Imm)}}$PC $4^{\ominus}$} (Figure 12, Supplemental Table 2) map to functional clusters which either (a) produce cytokines that impair other tissues' abilities to produce fluid or (b) propagate from the LG to other tissues, where they produce cytokines that impair fluid production.

As shown in Figure 5E, the mean STT-I_A score appeared to have decreased after systemic immunization, then increased in 2° ATD_{Imm} eyes after disease was adoptively transferred to the 1° ATD_{Imm} LG. Increasing STT-I_A scores in 2° ATD_{Imm} eyes were associated with increasing abundance of MHC II mRNA in 2° ATD_{Imm} LG (Figure 14C). Similar to the finding that immunization led to increases in STT-I scores in low IgG titer animals (Figure 4D, Figure 4G), this finding implies that variable sets {$^{2°\ ATD(Imm)}$PC $1^{\ominus}$}, {$^{2°\ ATD(Imm)}$PC $4^{\oplus}$}, {$^{2°\ ATD(Imm)}$PC $5^{\oplus}$}, and {$^{2°\ ATD(Imm)}$PC $6^{\ominus}$} (Figure 13, Supplemental Table 3) might map to functional clusters that express mediators which augment, rather than suppress, tear production.

I. Promoting Expression of Selected IMIP Phenotypes

Section III.H suggests that {$^{1°\ ATD(Imm)}$PC $1^{\ominus}$}, {$^{1°\ ATD(Imm)}$PC $1^{\oplus}$}, and {$^{1°\ ATD(Imm)}$PC $2^{\oplus}$} mapped to functional clusters that were associated with specific features of ocular surface and LG pathology. The transcript sets the functional clusters express include potential phenotype-specific therapeutic targets. If one were to plan studies to address these hypotheses, one would wish to promote development of functional clusters of interest. It appears that it may be possible to influence the incidence of LG with high or low levels of the {$^{1°\ ATD(Imm)}$PC $2^{\oplus}$} functional cluster vis à vis the {$^{1°\ ATD(Imm)}$PC $1^{\ominus}$} functional cluster. The results presented in Figure 15A indicate that increasing 1° ATD(Imm)PC $2^{\oplus}$ projections, i.e., increasing expression of variable set {$^{1°\ ATD(Imm)}$PC $2^{\oplus}$} expression, were associated with increasing PBL SI (R^2 = .697, *P*=.0387). As shown in Figure 4D increasing SI were associated with increasing initial immunizing P_i doses. Therefore, immunizing study animals with higher doses of P_i prior to adoptive transfer might increase the incidence of LG with high levels of {$^{1°\ ATD(Imm)}$PC $2^{\oplus}$} expression and atrophy associated with less fibrosis, less parenchymal disruption, but more lymphocytic infiltration, and the incidence of eyes with higher rose Bengal scores and lower STT-I_A scores. Linear regression analysis of the relationship between initial immunizing doses and 1° ATD(Imm)PC $2^{\oplus}$ projections (Figure 15B, R^2 = .628, *P*=.0603) suggests that this hypothesis deserves investigation.

The same reasoning predicts that it might be possible to promote the incidence of LG with atrophy associated with more fibrosis, more parenchymal disruption, and less lymphocytic infiltration and of eyes with lower rose Bengal staining scores and higher STT-IA scores if it were possible to decrease $^{1°\ ATD(Imm)}$PC 1 projections. Conversely, it might be possible to increase the incidence of LG with less atrophy but more ocular surface inflammation and lower STT-IA scores if it were possible to increase $^{1°\ ATD(Imm)}$PC 1 projections. $^{1°\ ATD(Imm)}$PC 1 projections were not found to be significantly associated with any of the experimental protocol variables nor with the magnitudes of the humoral or cellular autoimmune responses. Thus, like the humoral autoimmune responses (Figure 4A) $^{1°\ ATD(Imm)}$PC 1 projections appear to have been determined largely by intrinsic immunophysiological phenomena. In this context, it may be worth noting that decreasing $^{1°\ ATD(Imm)}$PC 3 projections were associated with increasing IgG titers (R^2 = .748, *P*=.0261) (Figure 15C). Accordingly, it might be possible to increase the expression of variable set {$^{1°\ ATD(Imm)}$PC $3^{\oplus}$} by selecting animals with low IgG titers and to increase the expression of variable set {$^{1°\ ATD(Imm)}$PC $3^{\ominus}$} by selecting animals with high IgG titers.

However, no significant associations between $^{1°\ ATD}$PC 3 projections and specific pathological features were detected.

IV. DISCUSSION

This report introduces novel protocols and autoantigen preparations for inducing experimental IMIP in the ocular surface tissues and LG. This report also illustrates the application of PCA as a tool to generate combinatorial models of functional cell clusters that describe diverse, multidimensional immunophysiological and pathological LG phenotypes. The implicit descriptions of predominant functional clusters' gene expression profiles both identify potential phenotype-specific therapeutic targets and point to the potential value of stratifying participants at the initiation of clinical trials. The findings presented demonstrate that intrinsic systemic and local immunophysiological variables interact with the experimental interventions to determine the expression of IMIP phenotypes ranging from relatively indolent to extremely severe, but they also suggest that it may be possible to design protocols to increase the incidence of selected IMIP phenotypes.

The use of mDC to activate the PBL makes adoptive transfer of IMIP to LG more efficiently practicable than previously described protocols, which employed autologous, primary cultured acinar cells as surrogate antigen presenting cells. Likewise, the use of prior immunization to exacerbate the severity of adoptively transferred IMIP is more efficient than previously described protocols, which required isolating autologous $CD4^+$ cells from MCR. Both innovations required identification of suitable autoantigen preparations. M_P, which LG acinar cells constitutively secrete to their underlying interstitial spaces, are compact packages containing both membrane phase and soluble phase autoantigens. Therefore, M_P may be a physiologically relevant autoantigen preparation for mDC-mediated activation of PBL. The P_i and S_i fractions can be readily isolated in larger quantities than M_P, and the P_i fraction can be more readily concentrated for high dose immunizing injections than the S_i fraction. Now that the efficacies of mDC-mediated PBL activation and prior immunization are established and PCA has been used to describe multidimensional IMID phenotypes, it might be informative to explore the IMIP phenotypes that arise when apoptotic cell debris, concentrated S_i, and reconstituted, concentrated P_i-S_i preparations are used as autoantigen sources.

The variability of PBL SI (Figure 3); the variability of humoral responses to immunization; and the variability of cellular responses to immunization (Figure 4) indicate the existence of underlying, intrinsic systemic immunophysiological variables that might influence the expression of adoptively transferred LG IMIP phenotypes and that also might influence the expression of natural LG IMIP phenotypes.

The variability of systemic immune responses in outbred populations is well known. Numerous genetic variables are being found to contribute. Differences between the MHC haplotypes of source animal mDC and study animal PBL may have been additional intrinsic sources of variability contributing to the observed differences in MCR SI of PBL from naïve animals. It should be noted, however, that the IMIP that were adoptively transferred in protocol 1 and protocol 3 were auto-immune, rather than alloimmune, as the activated PBL

which transferred disease were autologous. Moreover, the finding that the initial immunizing P_i dose significantly influenced MCR SI (Figure 4D) indicates that MHC mismatches were not the major source of SI variability among the PBL from the systemically immunized study animals.

Section III.H shows that variable sets $\{^{1^\circ\ ATD(Imm)}PC\ 1^{\ominus}\}$ and $\{^{1^\circ\ ATD(Imm)}PC\ 2^{\oplus}\}$ were associated with LG atrophy and suggested that $\{^{1^\circ\ ATD(Imm)}PC\ 1^{\ominus}\}$ might map to a functional cluster associated with more fibrosis and more parenchymal disruption while $\{^{1^\circ\ ATD(Imm)}PC\ 2^{\oplus}\}$ might map to a functional cluster associated with less fibrosis and less parenchymal disruption. Section III.I shows that it may be possible to promote expression of $\{^{1^\circ\ ATD(Imm)}PC\ 2^{\oplus}\}$ by immunizing animals with higher doses of P_i prior to adoptive transfer. Section III.I also shows that it might be possible to influence the incidence of the $\{^{1^\circ\ ATD(Imm)}PC\ 3^{\ominus}\}$ functional cluster *vis à vis* the $\{^{1^\circ\ ATD(Imm)}PC\ 3^{\oplus}\}$ functional cluster by selecting animals that had generated high or low IgG titers after systemic immunization. No experimental variable was found to have been significantly associated with the $\{^{1^\circ\ ATD(Imm)}PC\ 1^{\ominus}\}/\{^{1^\circ\ ATD(Imm)}PC\ 1^{\oplus}\}$ functional cluster dyad, suggesting that intrinsic immunophysiological variables exerted the predominant influence on the dyad.

As the $\{^{1^\circ\ ATD(Imm)}PC\ 1^{\ominus}\}/\{^{1^\circ\ ATD(Imm)}PC\ 1^{\oplus}\}$ functional cluster dyad is the major source of variability among the 1° ATD LG and the $\{^{1^\circ\ ATD(Imm)}\ Imm\ PC\ 1^{\ominus}\}$ functional cluster may be associated with a particular pattern of atrophy and histopathology, it will be of interest to elucidate the intrinsic variables that influences glands' $^{1^\circ\ ATD(Imm)}PC\ 1$ projections. Several findings suggest that they might related to a phenomenon which is both systematic and stochastic and which, paradoxically, is both adaptive and potentially pathogenic. Comparing the compositions of variable sets $\{^{Cont}PC\ 1^{\ominus}\}$, $\{^{1^\circ\ ATD(Imm)}PC\ 1^{\ominus}\}$, $\{^{1^\circ\ ATD(Imm)}PC\ 1^{\oplus}\}$, and $\{^{V(82\%29^\circ)}PC\ 1^{\ominus}\}$ (Section III.G.1 and Table 1), $\{^{Cont}PC\ 1^{\ominus}\}$ is largely homologous to $\{^{V(82\%29^\circ)}PC\ 1^{\ominus}\}$. $\{^{V(82\%29^\circ)}PC\ 1^{\ominus}\}$ was envisioned as mapping to an extended functional cluster ("network") that formed around a core functional cluster. The core cluster appears to develop systematically, in response to physiological signals related to environmental dryness, but the extent to which it develops in a given LG appears to be influenced by local, stochastic phenomena.[13] In addition to mRNAs for IL-4, IL-10, BAFF, CXCL13, CCL21, and CTLA-4, $\{^{V(82\%29^\circ)}PC\ 1^{\ominus}\}$ also includes mRNAs for IL-5, IL-7, IL-13, IL-21, CD25, CD86, CD19, and CD72 (Mircheff et al, unpublished). With such a transcript expression profile, the $\{^{V(82\%29^\circ)}PC\ 1^{\ominus}\}$ functional cluster is reminiscent of an ectopic lymphoid structure capable of recruiting immature B cells and resting T cells, supporting T cell survival, and supporting B cell activation and differentiation. The suggestion that the $\{^{V(82\%29^\circ)}PC\ 1^{\ominus}\}$ functional cluster may have adaptive value stems from its evident pro-T_H2 and pro-T_R1 character, which should counteract the ability of pathogenic T_H1 cells to propagate IMIP to the LG from other sites. The suggestion that it is potentially pathogenic stems from a theoretical prediction that it expands exponentially over time to eventually manifest as a pathological infiltrate. $\{^{1^\circ\ ATD(Imm)}PC\ 1^{\oplus}\}$ includes 13 of the $\{^{Cont}PC\ 1^{\ominus}\}$ variables, and $\{^{1^\circ\ ATD(Imm)}PC\ 1^{\oplus}\}$ includes 5 of the $\{^{Cont}PC\ 1^{\ominus}\}$ variables. These considerations suggest that the extent to which the $\{^{Cont}PC\ 1^{\ominus}\}$ functional cluster had developed prior to adoptive transfer influenced the direction in which it evolved after adoptive transfer. Therefore, it may be possible to promote or suppress development of the

{$^{1°\ ATD(Imm)}$PC $1^{\oplus}$} functional cluster by preconditioning study animals at higher or lower degrees of dryness.

As noted in Section III.I, the set of transcripts a functional cluster expresses includes potentially productive therapeutic targets, and it also identifies potential targets that are not likely to be productive. The functional clusters that express mRNAs for IL-6, IL-17A, and IL-18 illustrate this hypothesis. IL-6 mRNA is of interest because increases in its abundance were associated with decreasing STT-I_A scores in 1° ATD eyes. IL-6 mRNA was expressed by the {$^{1°\ ATD(Imm)}$PC $1^{\ominus}$}, $^{1°\ ATD(Imm)}$PC $2^{\oplus}$}, and $^{1°\ ATD(Imm)}$PC $4^{\ominus}$} functional clusters. Thus, drugs or biologicals that target IL-6 might be effective for aqueous tear deficiency phenotypes dominated by the {$^{1°\ ATD(Imm)}$PC $1^{\ominus}$}, {$^{1°\ ATD(Imm)}$PC $2^{\oplus}$}, and {$^{1°\ ATD(Imm)}$PC $4^{\ominus}$} functional clusters. Conversely, such modalities might not impact IMIP phenotypes dominated by the {$^{1°\ ATD(Imm)}$PC $1^{\oplus}$}, {$^{ATD(Imm)}$PC $2^{\ominus}$}, or {$^{1°\ ATD(Imm)}$PC $4^{\oplus}$} functional clusters. Likewise, IL-17A mRNA was expressed by the {$^{1°\ ATD(Imm)}$PC $1^{\oplus}$}, {$^{1°\ ATD(Imm)}$PC $2^{\oplus}$}, and {$^{1°\ ATD(Imm)}$PC $5^{\oplus}$} functional clusters. Thus, drugs or biologicals that target IL-17A would not be expected to impact IMIP phenotypes dominated by the {$^{1°\ ATD(Imm)}$PC $1^{\ominus}$}, {$^{ATD(Imm)}$PC $2^{\ominus}$}, or {$^{1°\ ATD(Imm)}$PC $5^{\ominus}$} functional clusters. Similarly, IL-18 mRNA was expressed by the {$^{1°\ ATD(Imm)}$PC $1^{\ominus}$}, {$^{1°\ ATD(Imm)}$PC $2^{\oplus}$}, {$^{1°\ ATD(Imm)}$PC $3^{\oplus}$}, or {$^{1°\ ATD(Imm)}$PC $4^{\ominus}$} functional clusters. Thus, drugs or biologicals that target IL-18 would not be expected to impact IMIP phenotypes dominated by the {$^{1°\ ATD(Imm)}$PC $1^{\oplus}$}, {$^{1°\ ATD(Imm)}$PC $2^{\ominus}$}, {$^{1°\ ATD(Imm)}$PC $3^{\ominus}$}, and {$^{1°\ ATD(Imm)}$PC $4^{\oplus}$} functional clusters. This same reasoning suggests that stratifying participants according to disease phenotype at the outset of a clinical trial might improve the chances of demonstrating the efficacy of a modality that targets a subset of LG IMIP phenotypes.

The exigencies of pharmacodynamic and pharmacokinetic distribution studies demand rabbits and other models of similar or larger size. Empirical findings[35] and theoretical considerations[36] suggest that cellular and molecular immunological mechanisms in some larger animal models should mimic the cognate mechanisms in humans more closely than do the mechanisms in mouse models, which otherwise are ideally suited for immunological studies. The present findings point to an urgent need to understand the underlying, immunopathological diversity of the IMIP phenotypes that arise in patients. In view of the evidence that it will possible to modulate IMIP phenotype expression in animal models, it may be possible to develop models that adequately mimic specific human IMIP phenotypes. Such models might accelerate identification and validation of effective new therapies.

V. CONCLUSIONS

LG manifest diverse immunohomeostatic phenotypes, likely influenced by interactions between intrinsic, stochastic phenomena, determined responses to environmental exposures, and physiological hormonal changes. Intrinsic phenomena, some related to systemic immunophysiological variables, others apparently related to glands' initial immunohomeostatic phenotypes, interact with the novel autoantigen preparations and protocols that have been introduced to determine expression of LG IMIP phenotypes, which range from relatively indolent to extremely severe. PCA appears to be a useful tool for constructing combinatorial, cellular and molecular, models of LG immunohomeostatic and

IMIP phenotypes. Knowledge about the IMIP phenotypes that arise in individual patients may help guide the search for effective therapeutics and the design of clinical trials.

Supplementary Material

Refer to Web version on PubMed Central for supplementary material.

ACKNOWLEDGMENTS

The authors thank Dr. Wendy Gilmore, Keck School of Medicine, for many thoughtful discussions.

Supported by an unrestricted grant from Allergan (AKM) and NIH Grant DK 048522.

REFERENCES

1. Bron AJ, Yokoi N, Gafney E, Tiffany JM. Predicted phenotypes of dry eye: proposed consequences of its natural history. Ocul Surf. 2009; 7:78–92. [PubMed: 19383277]
2. Lemp MA, Crews LA, Bron AJ, et al. Distribution of aqueous-deficient and evaporative dry eye in a clinic-based patient cohort: A retrospective study. Cornea. 2012; 31:472–8. [PubMed: 22378109]
3. Damato BE, Allan D, Murray SB, Lee WR. Senile atrophy of the human lacrimal gland: the contribution of chronic inflammatory disease. Br J Ophthalmol. 1984; 68:674–80. [PubMed: 6331845]
4. Khanal S, Tomlinson A. Tear physiology in dry eye associated with chronic GVHD. Bone Marrow Transplant. 2012; 47:115–9. [PubMed: 21383687]
5. Christodoulou MI, Kapsogeorgou EK, Moutsopoulos HM. Characteristics of the minor salivary gland infiltrates in Sjögren's syndrome. J Autoimmun. 2010; 34:400–7. [PubMed: 19889514]
6. Kapsogeorgou EK, Christodoulou MI, Panagiotakos DB, et al. Minor salivary gland inflammatory lesions in Sjögren's syndrome: do they evolve? J Rheumatol. 2013; 40:1566–71. [PubMed: 23908448]
7. Lemp MA. Report of the National Eye Institute/Industry workshop on Clinical Trials in Dry Eyes. CLAO J. 1995; 21:221–32. [PubMed: 8565190]
8. Waterhouse JP. Focal adenitis in salivary and lacrimal glands. Proc R Soc Med. 1963; 56:911–7. [PubMed: 14068151]
9. Obata H, Yamamoto S, Horiuchi H, Machinami R. Histopathologic study of human lacrimal gland. Statistical analysis with special reference to aging. Ophthalmology. 1995; 102:678–86. [PubMed: 7724184]
10. Novack GP. Why aren't there more pharmacotherapies for dry eye? Ocul Surf. 2014; 12:227–9. [PubMed: 24999105]
11. de Saint Jean M, Nakamura T, Wang Y, et al. Suppression of lymphocyte proliferation and regulation of dendritic cell phenotype by soluble mediators from rat lacrimal epithelial cells. Scand J Immunol. 2009; 70:53–62. [PubMed: 19522768]
12. Mircheff AK, Wang Y, de St Jean M, et al. Mucosal immunity and self tolerance in the ocular surface system. Ocul Surf. 2005; 3:182–92. [PubMed: 17131026]
13. Mircheff AK, Wang Y, Ding C, et al. Potentially pathogenic immune cells and networks in apparently healthy lacrimal glands. Ocul Surf. 2015; 13:47–81. [PubMed: 25557346]
14. Zhu Z, Stevenson D, Schechter JE, et al. Lacrimal histopathology and ocular surface disease in a rabbit model of autoimmune dacryoadenitis. Cornea. 2003; 22:25–32. [PubMed: 12502944]
15. Thomas PB, Zhu Z, Selvam S, et al. Autoimmune dacryoadenitis and keratoconjunctivitis induced in rabbits by subcutaneous injection of autologous lymphocytes activated ex vivo against lacrimal antigens. J Autoimmun. 2008; 31:116–22. [PubMed: 18534818]
16. Wei RH, Thomas PB, Samant DM, et al. Autoimmune dacryoadenitis and sialadenitis induced in rabbits by intravenous injection of autologous lymphocytes activated ex vivo against lacrimal antigens. Cornea. 2012; 31:693–701. [PubMed: 22333667]

17. Thomas PB, Samant DM, Wang Y, et al. Distinct dacryoadenitides autoadoptively transferred to rabbits by different subpopulations of lymphocytes activated ex vivo. Cornea. 2010; 29:1153–62. [PubMed: 20577087]
18. Guo Z, Azzarolo AM, Schechter JE, et al. Lacrimal gland epithelial cells stimulate proliferation in autologous lymphocyte preparations. Exp Eye Res. 2000; 71:11–22. [PubMed: 10880272]
19. Gierow JP, Lambert RW, Mircheff AK. Fluid phase endocytosis by isolated rabbit lacrimal gland acinar cells. Exp Eye Res. 1995; 60:511–25. [PubMed: 7615017]
20. Cody V, Shen H, Shlyankevich M, et al. Generation of dendritic cells from rabbit bone marrow mononuclear cell cultures supplemented with hGM-CSF and hIL-4. Vet Immunol Immunopathol. 2005; 103:163–72. [PubMed: 15621303]
21. Thomas PB, Samant DM, Selvam S, et al. Adeno-associated virus-mediated IL-10 gene transfer suppresses lacrimal gland immunopathology in a rabbit model of autoimmune dacryoadenitis. Invest Ophthalmol Vis Sci. 2010; 51:5137–44. [PubMed: 20505195]
22. Guo Z, Song D, Azzarolo ZM, et al. Autologous lacrimal-lymphoid mixed-cell reactions induce dacryoadenitis in rabbits. Exp Eye Res. 2000; 71:23–31. [PubMed: 10880273]
23. Ohyama K, Baba M, Tamai M, et al. Proteomic profiling of antigens in circulating immune complexes associated with each of seven autoimmune diseases. Clin Biochem. 2015; 48:181–5. [PubMed: 25438073]
24. Szodoray P, Koczok K, Szanto A, et al. Autoantibodies to novel membrane and cytosolic antigens of the lachrymal gland in primary Sjögren's syndrome. Clin Rheumatol. 2008; 27:195–9. [PubMed: 17713716]
25. Grus FH, Dick B, Augustin AJ, Pfeiffer N. Analysis of the antibody repertoire in tears of dry-eye patients. Ophthalmologica. 2001; 215:430–4. [PubMed: 11741110]
26. Dick AD, Cheng YF, McKinnon A, et al. Nasal administration of retinal antigens suppresses the inflammatory response in experimental allergic uveoretinitis. A preliminary report of intranasal induction of tolerance with retinal antigens. Br J Ophthalmol. 1993; 77:171–5. [PubMed: 8457510]
27. Ringnér M. What is principal component analysis? Nat Biotechnol. 2008; 26:303–4. [PubMed: 18327243]
28. Armstrong NJ, van de Wiel MA. Microarray data analysis: from hypotheses to conclusions using gene expression data. Cell Oncol. 2004; 26:279–90. [PubMed: 15623938]
29. Ma S, Kosorok MR. Identification of differential gene pathways with principal component analysis. Bioinformatics. 2009; 25:882–9. [PubMed: 19223452]
30. Morris DL, Vyse TJ. Analysis of systemic lupus erythematosus subphenotype data for genetic association. Curr Opin Rheumatol. 2012; 24:482–8. [PubMed: 22732687]
31. Hsu FC, Kritchevsky SB, Liu Y, et al. Association between inflammatory components and physical function in the health, aging, and body composition study: a principal component analysis approach. J Gerontol A Biol Sci Med Sci. 2009; 64:581–9. [PubMed: 19228783]
32. Perou CM, Sørlie T, Eisen MB, et al. Molecular portraits of human breast tumours. Nature. 2000; 406(6797):747–52. [PubMed: 10963602]
33. Maitchouk DY, Beuerman RW, Ohta T, et al. Tear production after unilateral removal of the main lacrimal gland in squirrel monkeys. Arch Ophthalmol. 2000; 118:246–52. [PubMed: 10676790]
34. Selvam S, Mircheff AK, Yiu SC. Diverse mediators modulate the chloride ion fluxes that drive lacrimal fluid production. Invest Ophthalmol Vis Sci. 2013; 54:2927–33. [PubMed: 23513060]
35. Schechter JE, Warren DW, Mircheff AK. A lacrimal gland is a lacrimal gland, but rodent's and rabbit's are not human. Ocul Surf. 2010; 8:111–34. [PubMed: 20712969]
36. Dawson, HD. A comparative assessment of the pig, mouse, and human genomes: structural and functional analysis of genes involved in immunity and inflammation. In: McAnulty, PA.; Dayan, AD.; Ganderup, N-C.; Hastings, KL., editors. The Minipig in Biomedical Research. CRC Press, Taylor & Francis Group; 2011. p. 321-41.

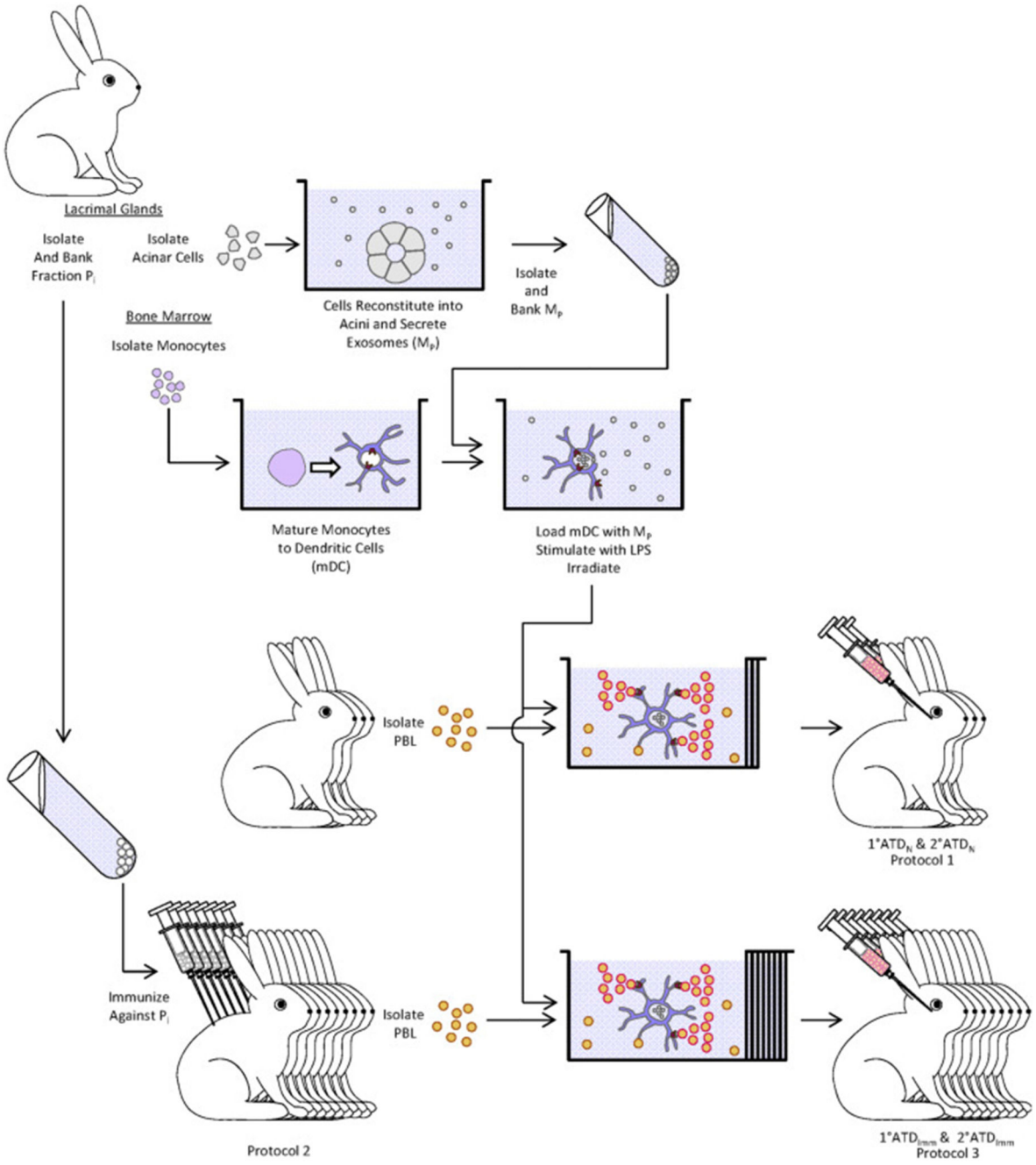

Figure 1.
Overview of experimental protocols.

Figure 2.
Western blots of Pi, Si, and MP were probed with serum from a diseased female NOD mouse and secondary antibody to mouse IgG.

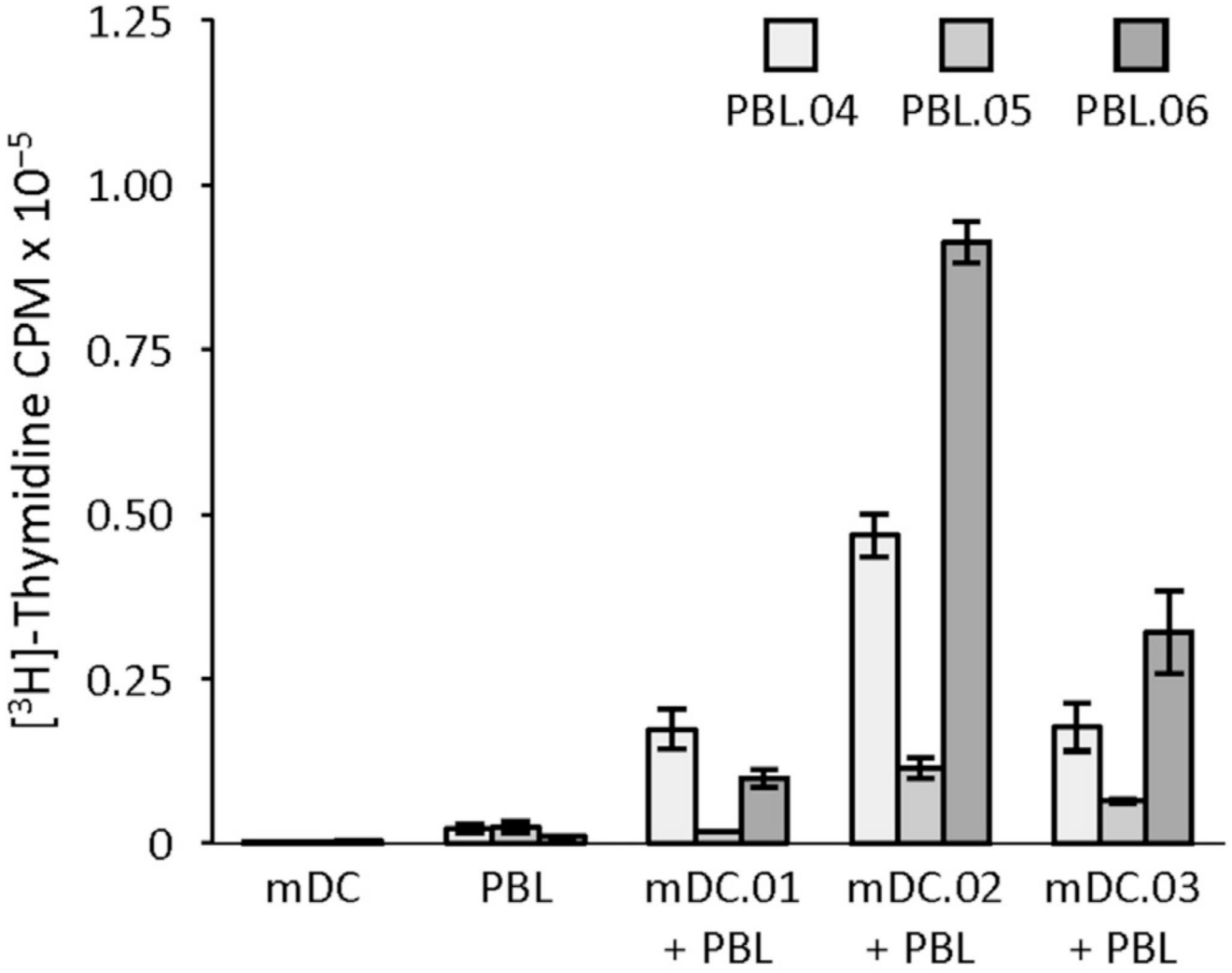

Figure 3.
Mixed cell reactions between mDC from animals 01, 02, and 03 and PBL from animals 04, 05, and 06.

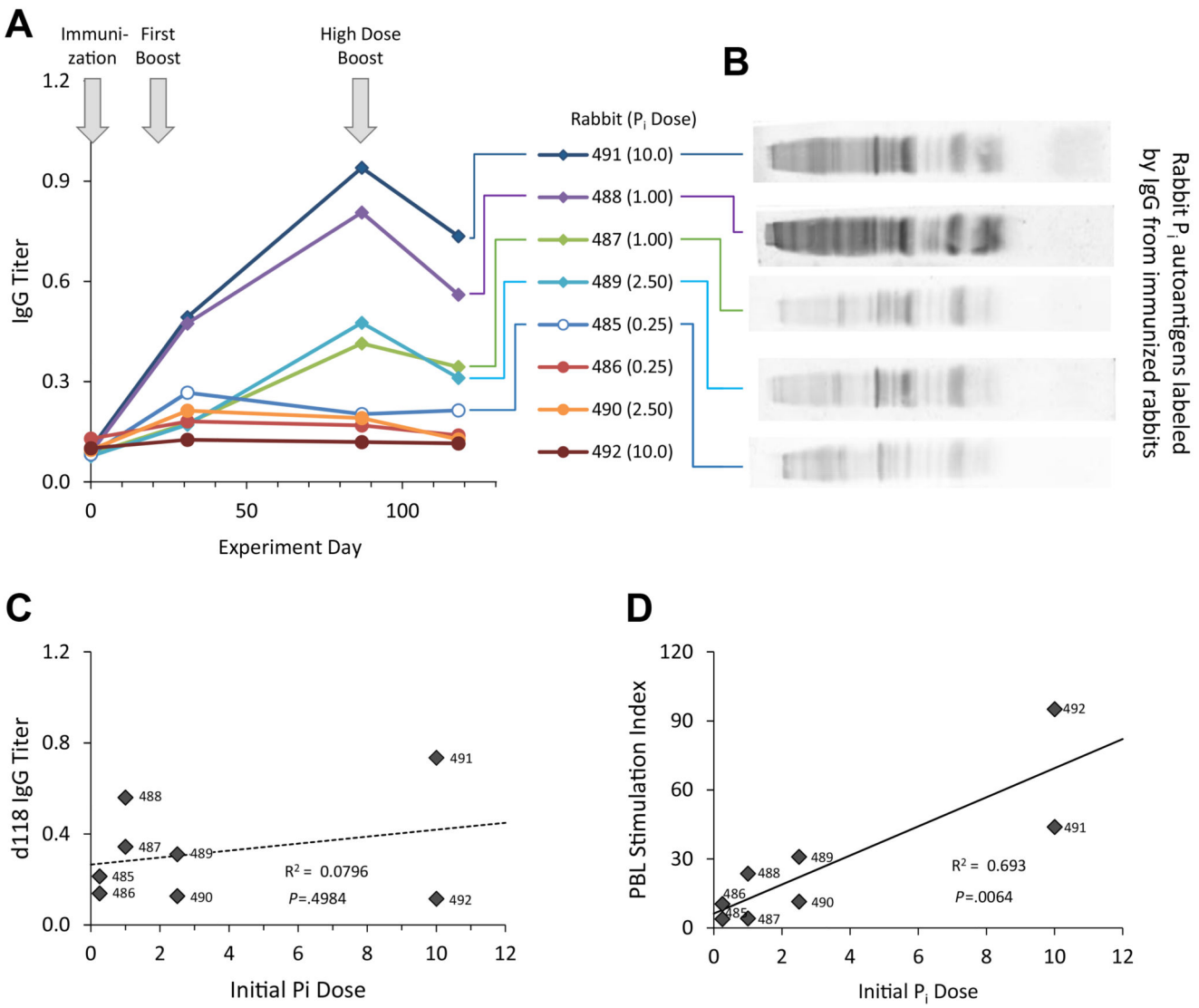

Figure 4.

Humoral autoimmune responses after systemic immunization with Pi. (A) Time-courses of IgG titers detected by ELISA. (B) Western blots of identical aliquots of MP were probed with sera from the immunized animals, then probed with secondary antibody. Blots shown were probed with sera with 5 highest IgG titers and strongest Western blot signals. Signals from blots probed only with secondary antibody were undetectable at the settings used. (C) Plot of day 118 IgG titers indicates no simple association with initial immunizing Pi doses. (D) PBL stimulation indices appear to have been significantly influenced by initial immunizing Pi doses.

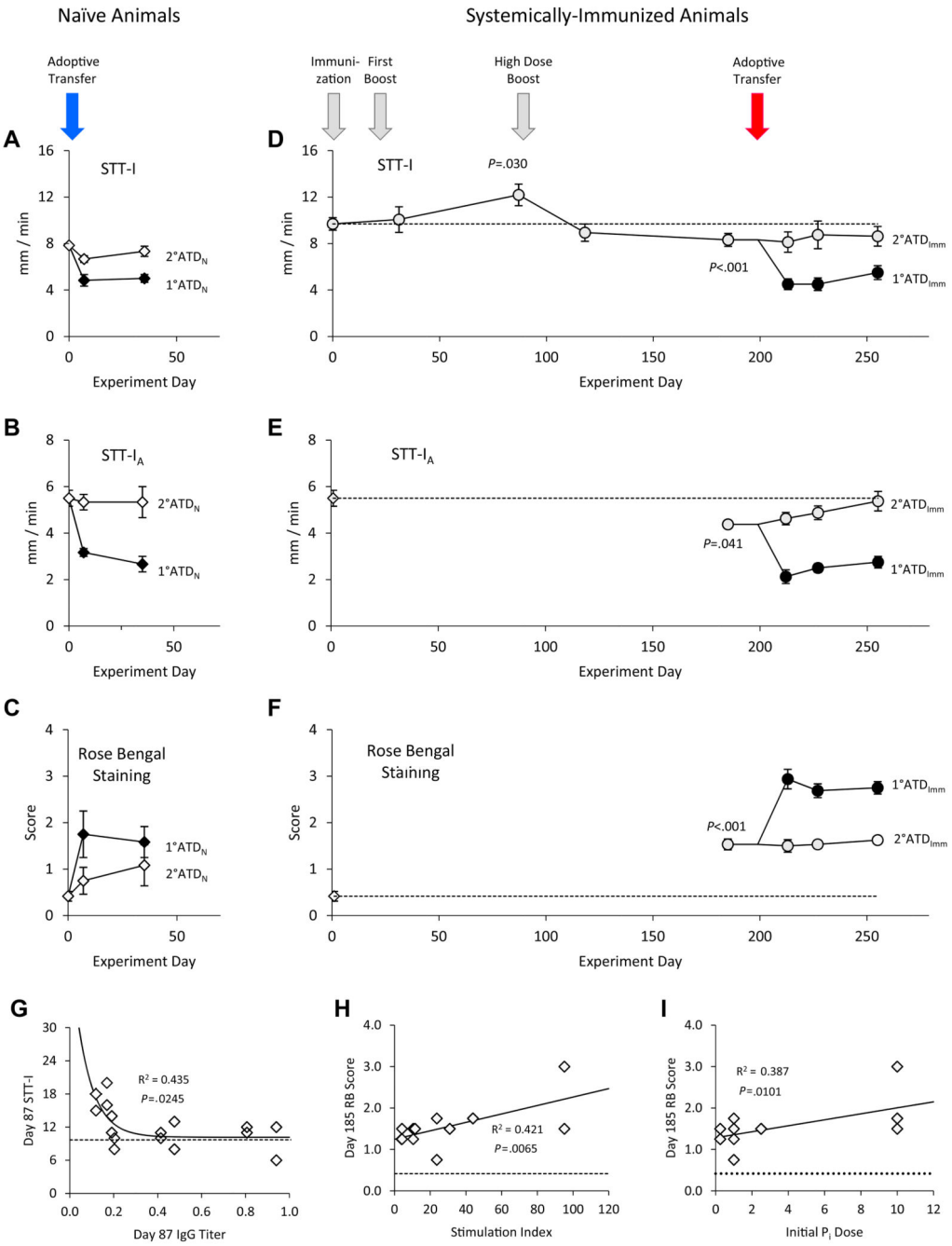

Figure 5.

Ocular surface manifestations. (A, B, and C) STT-I, STT-IA, and rose Bengal staining scores at baseline and over time after activated PBL were after adoptively transferred to OD LG of naïve animals. (D, E, and F) STT-I, STT-IA, and rose Bengal staining scores at baseline, over time after systemic immunization, and over time after activated PBL were after adoptively transferred to OD LG of the systemically immunized animals. (G) Relationship between day 87 STT-I scores and day 87 IgG titers. Dashed line indicates mean baseline value. (H) Relationship between day 185 rose Bengal scores and stimulation indices

(measured on day 199). Dashed line indicates mean baseline values. (I) Relationship between day 185 rose Bengal scores and initial immunizing Pi dose.

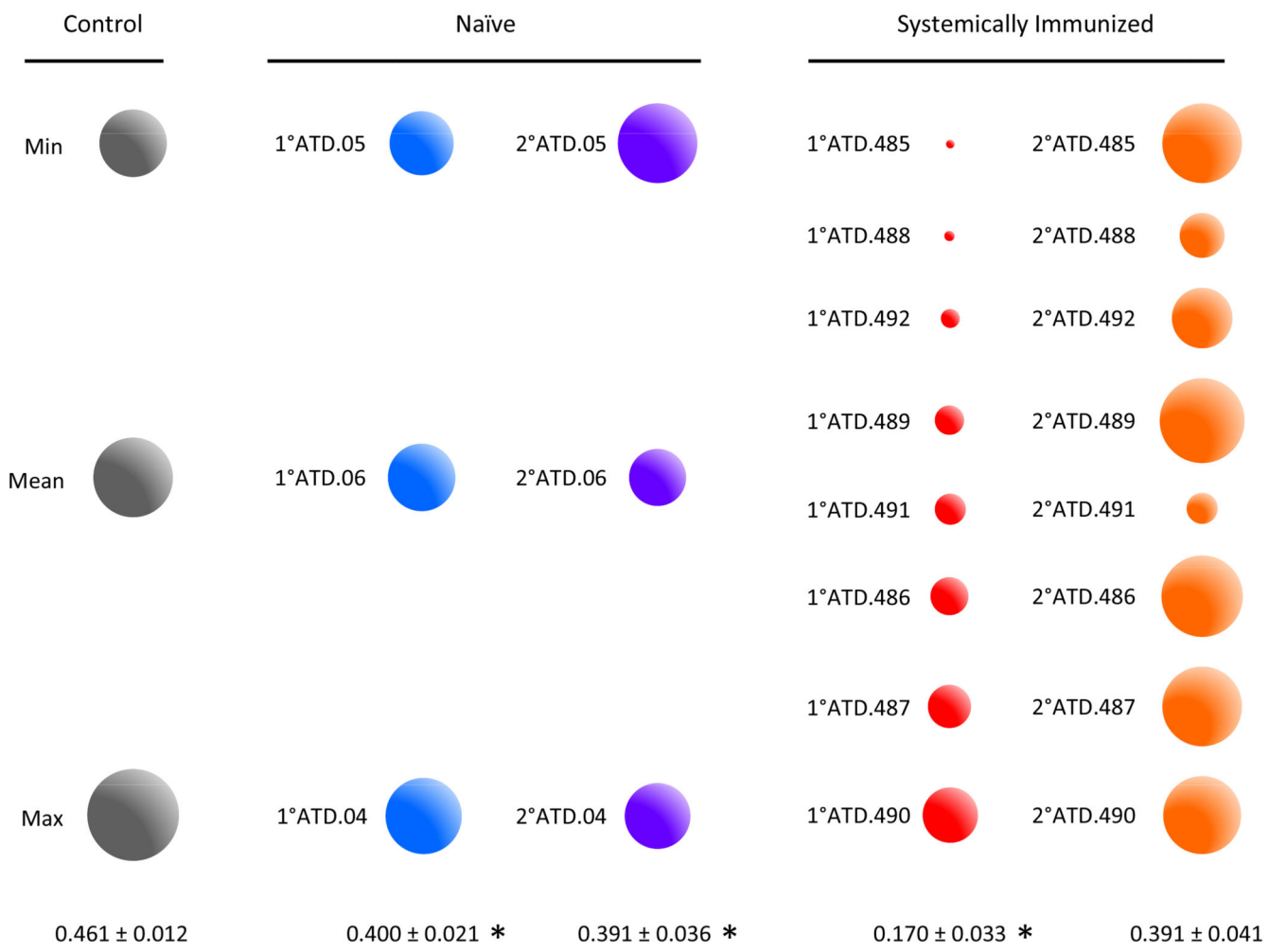

Figure 6.

RNA yields as surrogate markers of glandular survival. Volumes of spheres are proportional to RNA yields. Values presented are mean ± sem for each group of LG. *Indicates *P* for difference from control <.05.

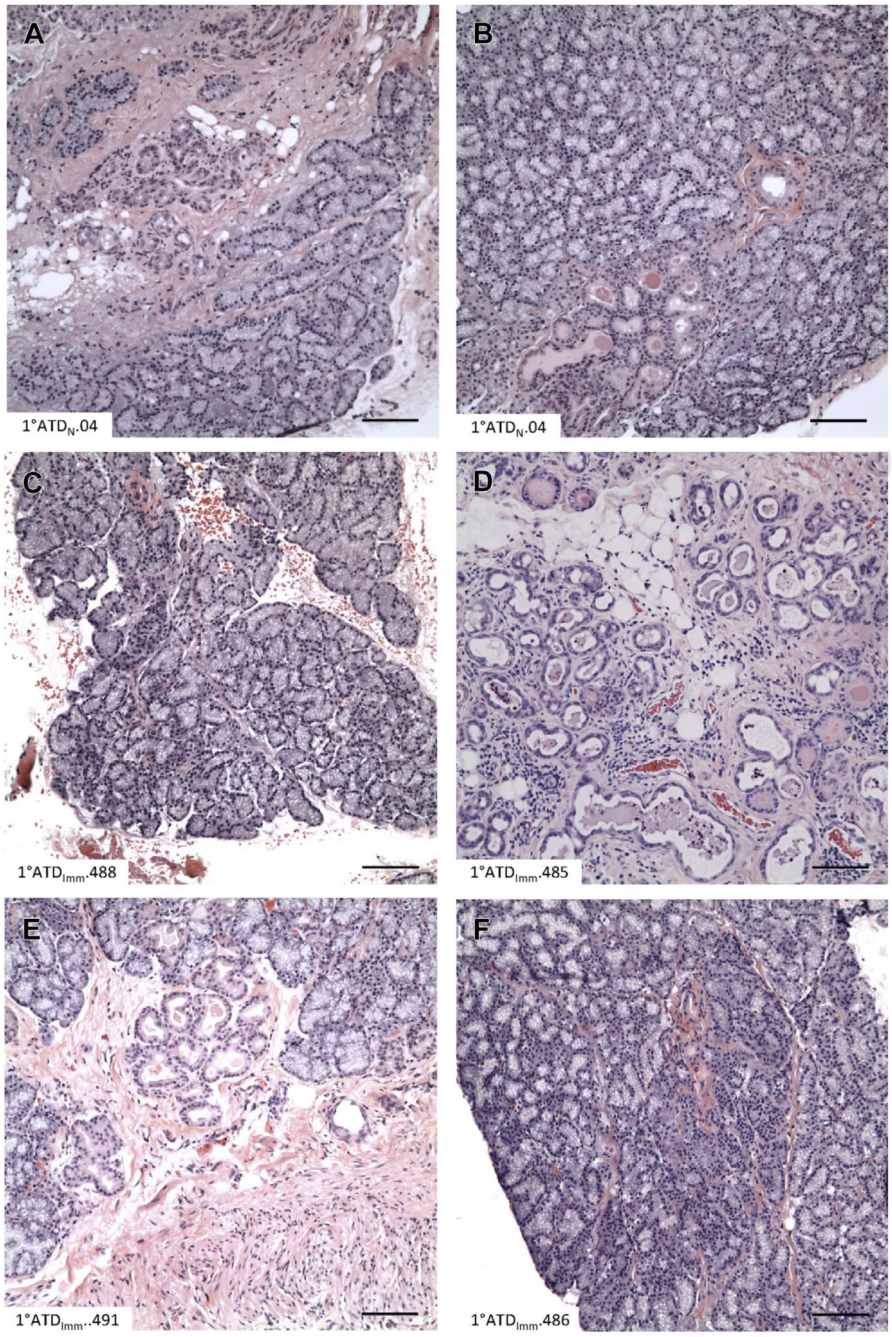

Figure 7.

Images of H&E stained sections of 1° ATD glands from naïve animals and systemically immunized animals. Bars = 100 μ. Magnification = 20×.

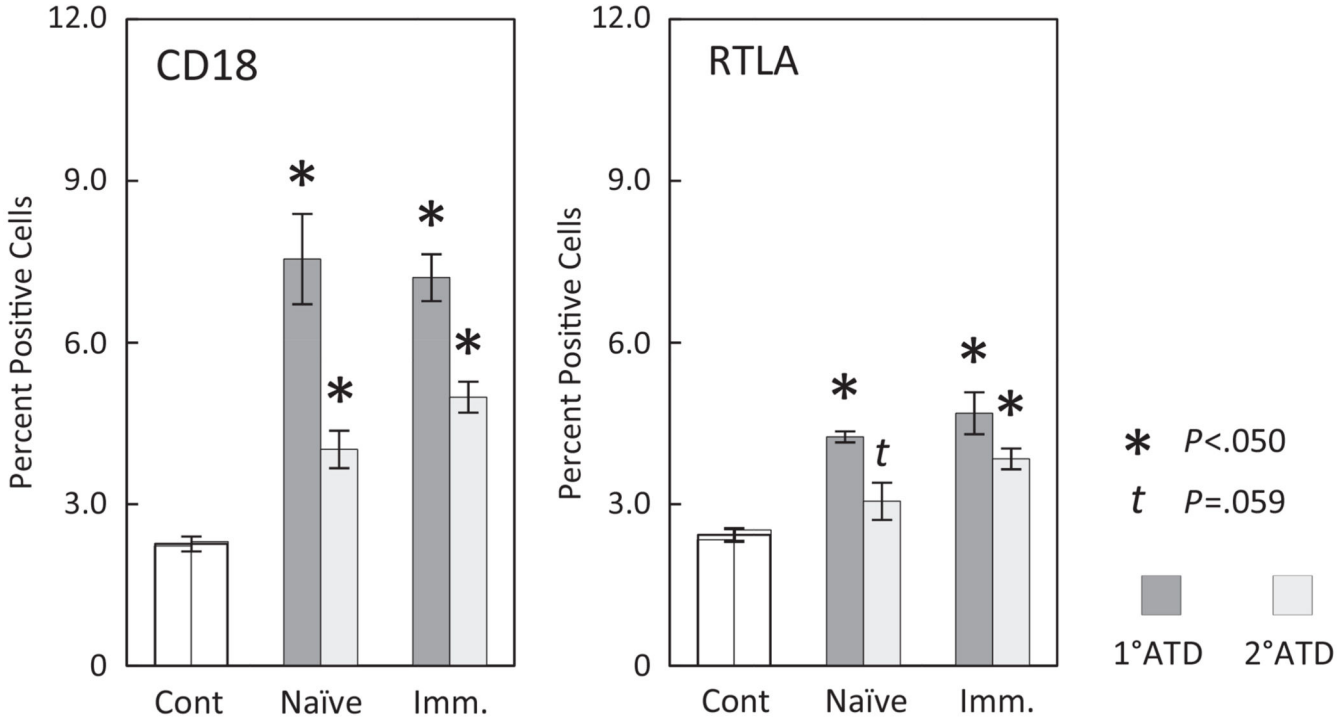

Figure 8.

Quantitation of CD18+ and RTLA+ cells in glands from control animals; 1° ATD- and 2° ATD glands from naïve animals; and 1° ATD- and 2° ATD glands from animals that had been systemically immunized with Pi before adoptive transfer of activated PBL.

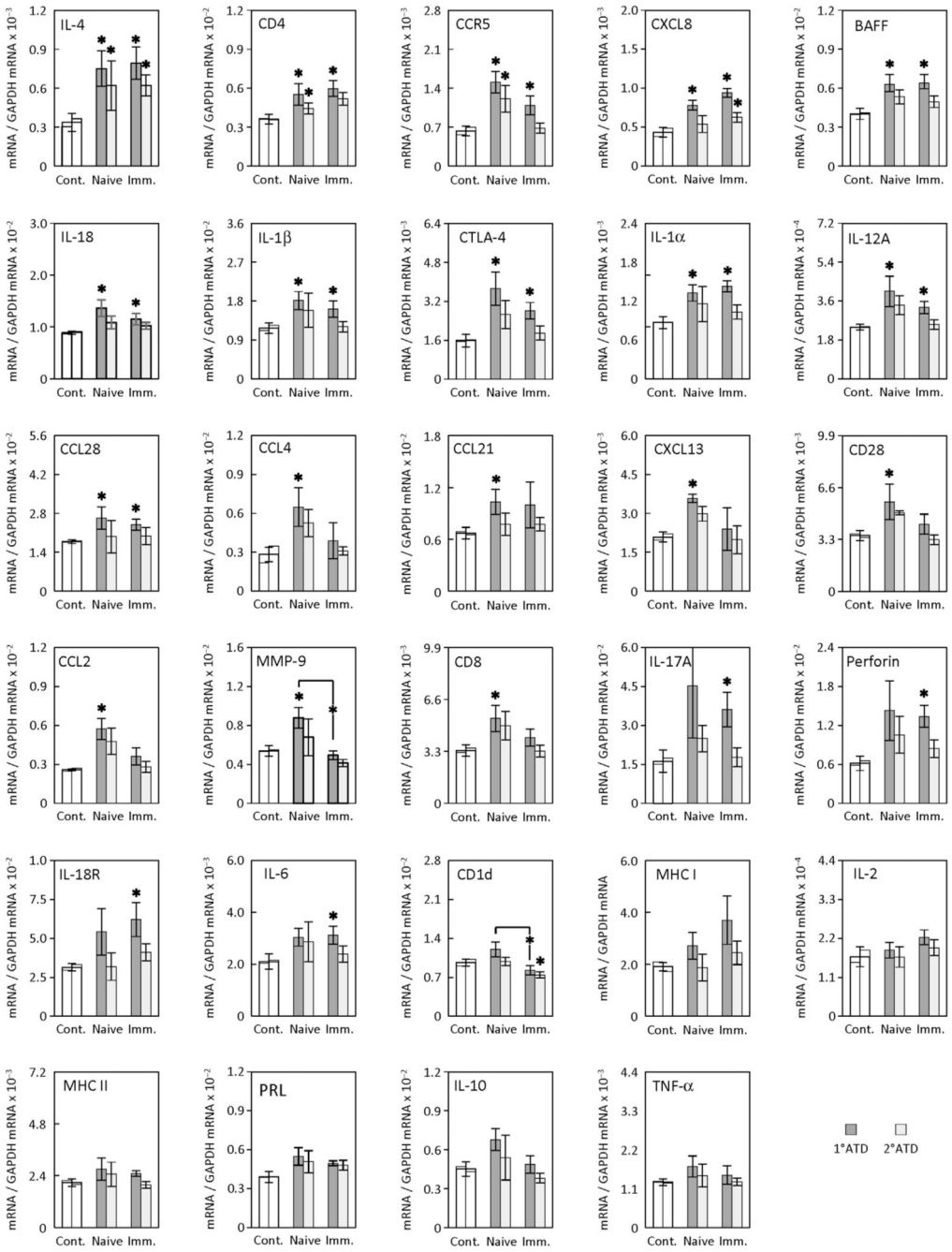

Figure 9.

Immune response-related gene transcript abundances in glands from control animals; 1° ATD and 2° ATD glands from naïve animals; and 1° ATD- and 2° ATD glands from animals that had been systemically immunized with Pi before adoptive transfer of activated PBL.

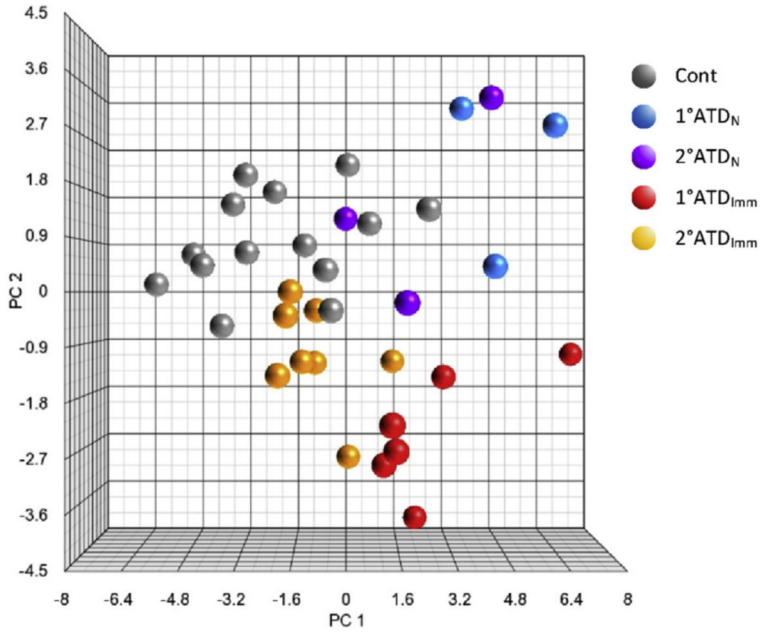

	PC 1	PC 2
1°ATD$_N$ vs. Cont	<0.001	0.055
2°ATD$_N$ vs. Cont	0.013	-
1°ATD$_{Imm}$ vs. Cont	<0.001	<0.001
2°ATD$_{Imm}$ vs. Cont	-	0.001
1°ATD$_N$ vs. 2°ATD$_N$	-	-
1°ATD$_{Imm}$ vs. 2°ATD$_{Imm}$	0.019	0.03
1°ATD$_N$ vs. 1°ATD$_{Imm}$	-	<0.001
1°ATD$_N$ vs. 2°ATD$_{Imm}$	<0.001	<0.001
2°ATD$_N$ vs. 1°ATD$_{Imm}$	-	<0.001
2°ATD$_N$ vs. 2°ATD$_{Imm}$	0.015	0.005

Figure 10.

Principal component analysis the LG from the control and 4 experimental LG groups. The 3-dimensional scatterplot presents the individual glands' PC 1, PC 2, and PC 3 projections. As abundances of mRNAs for IL 2 and IL 4 were undetermined in 2 of the control LG and in 1° ATD LG.492, these transcripts were not included in the analyses. The inset presents *P* values for pairwise comparisons of mean PC 1 and PC 2 projections. Differences between mean PC 3 projections were not statistically significant.

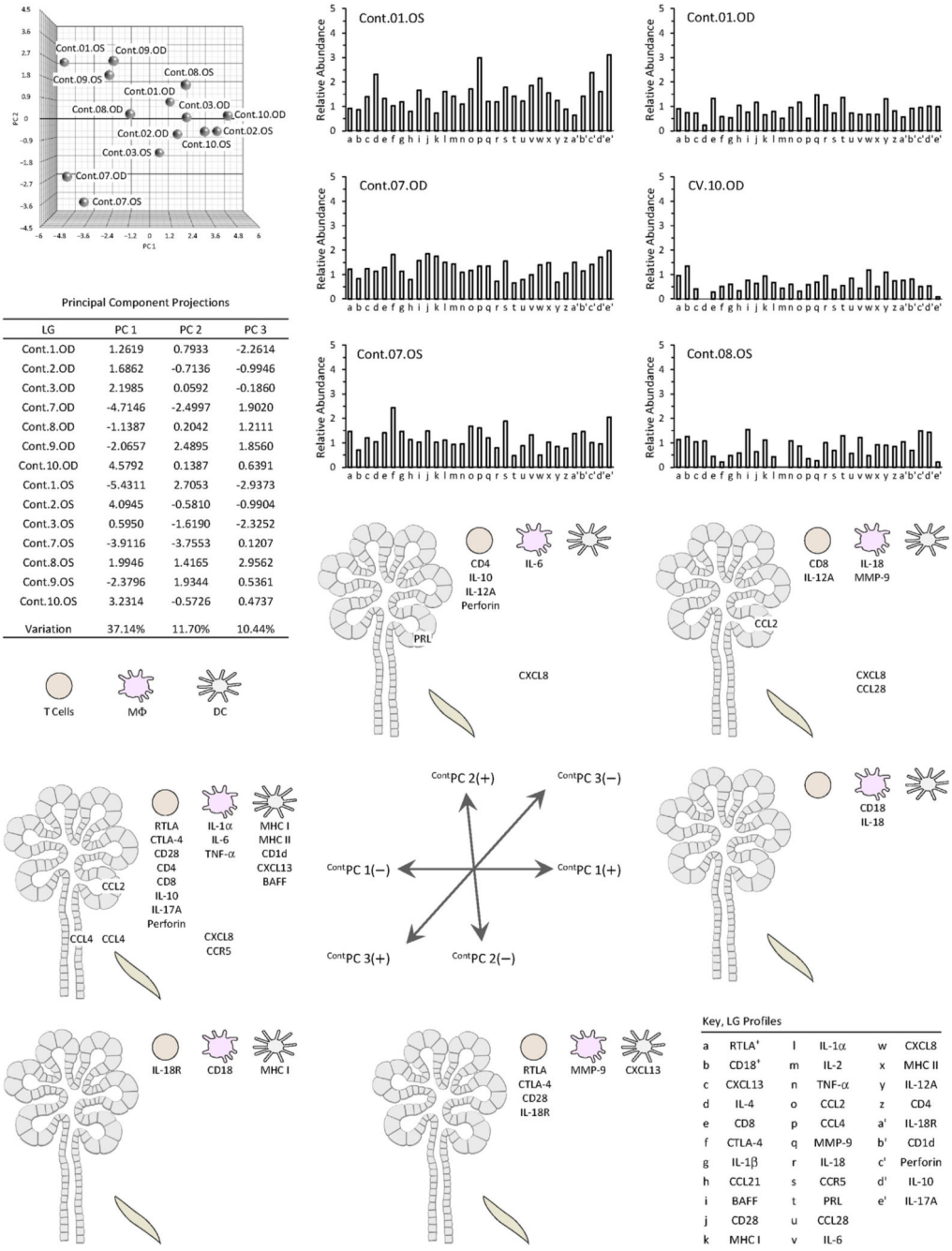

Principal Component Projections

LG	PC 1	PC 2	PC 3
Cont.1.OD	1.2619	0.7933	-2.2614
Cont.2.OD	1.6862	-0.7136	-0.9946
Cont.3.OD	2.1985	0.0592	-0.1860
Cont.7.OD	-4.7146	-2.4997	1.9020
Cont.8.OD	-1.1387	0.2042	1.2111
Cont.9.OD	-2.0657	2.4895	1.8560
Cont.10.OD	4.5792	0.1387	0.6391
Cont.1.OS	-5.4311	2.7053	-2.9373
Cont.2.OS	4.0945	-0.5810	-0.9904
Cont.3.OS	0.5950	-1.6190	-2.3252
Cont.7.OS	-3.9116	-3.7553	0.1207
Cont.8.OS	1.9946	1.4165	2.9562
Cont.9.OS	-2.3796	1.9344	0.5361
Cont.10.OS	3.2314	-0.5726	0.4737
Variation	37.14%	11.70%	10.44%

Figure 11.

Principal component analysis of the LG from control glands animals. Inset charts present immune cell number- and transcript abundance profiles of selected LG. Values are normalized to the mean values in control glands. Inset table presents the individual LG's PC 1, PC 2, and PC 3 projections. Illustrations depict the proposed functional cluster models for the PC 1, PC 2, and PC 3 dyads; the epithelial cell types (acinar or ductal) that were found to express mRNAs for CCL2, CCL4, and PRL[13]; and the immune and stromal cell types that typically express the listed transcripts.

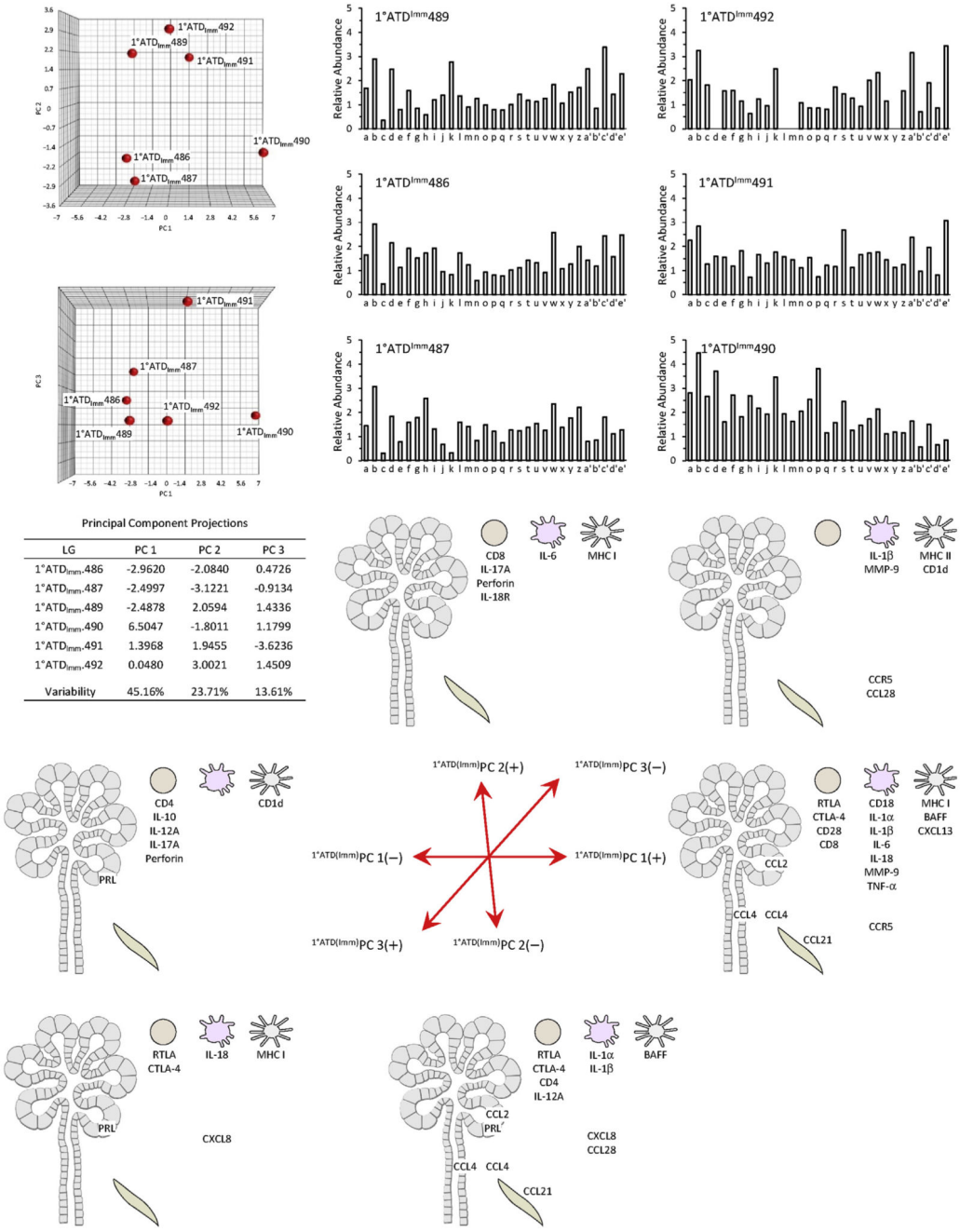

Principal Component Projections

LG	PC 1	PC 2	PC 3
1°ATD$_{Imm}$.486	-2.9620	-2.0840	0.4726
1°ATD$_{Imm}$.487	-2.4997	-3.1221	-0.9134
1°ATD$_{Imm}$.489	-2.4878	2.0594	1.4336
1°ATD$_{Imm}$.490	6.5047	-1.8011	1.1799
1°ATD$_{Imm}$.491	1.3968	1.9455	-3.6236
1°ATD$_{Imm}$.492	0.0480	3.0021	1.4509
Variability	45.16%	23.71%	13.61%

Figure 12.
Principal component analysis of the 1° ATDImm LG.

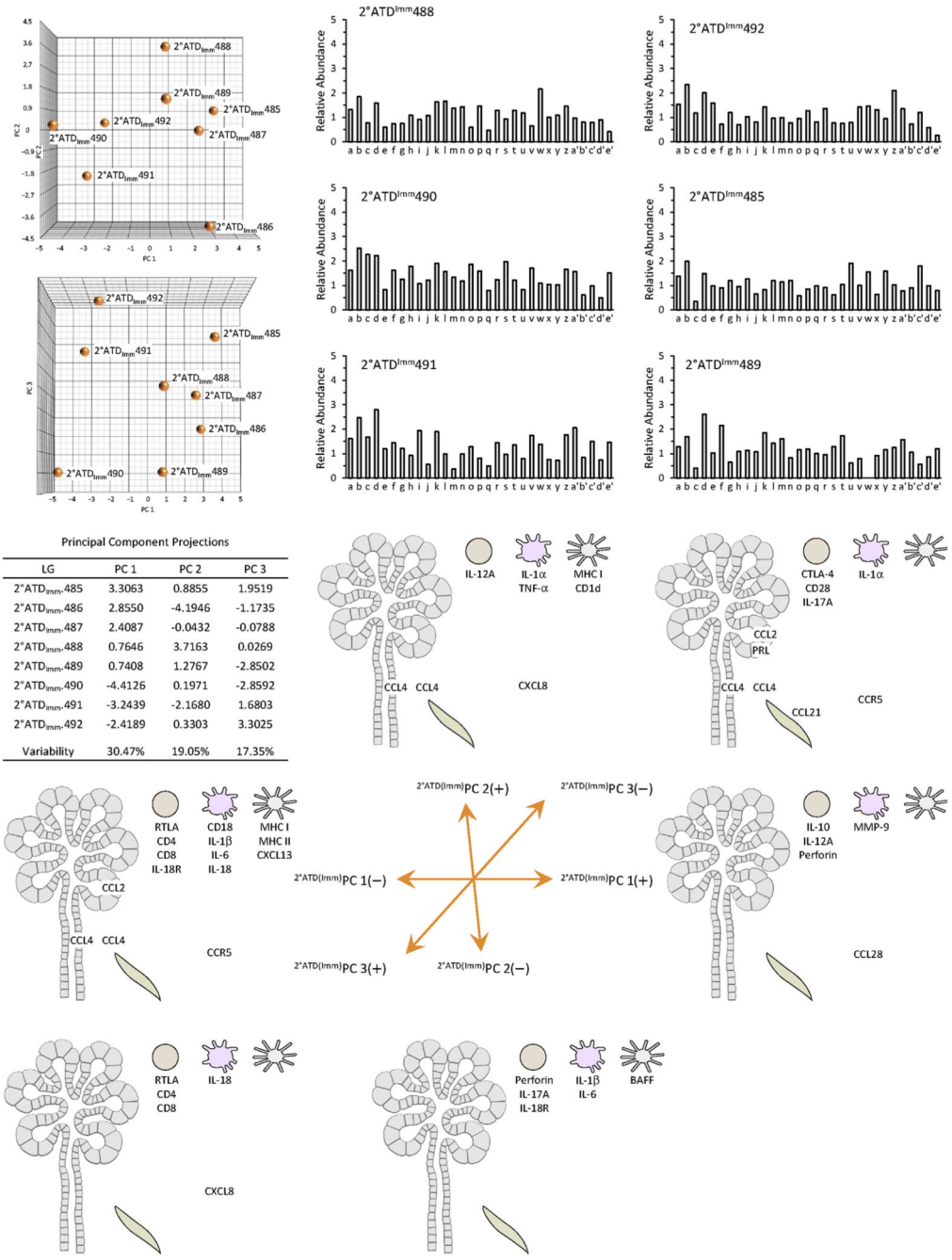

Principal Component Projections

LG	PC 1	PC 2	PC 3
2°ATD$_{Imm}$.485	3.3063	0.8855	1.9519
2°ATD$_{Imm}$.486	2.8550	-4.1946	-1.1735
2°ATD$_{Imm}$.487	2.4087	-0.0432	-0.0788
2°ATD$_{Imm}$.488	0.7646	3.7163	0.0269
2°ATD$_{Imm}$.489	0.7408	1.2767	-2.8502
2°ATD$_{Imm}$.490	-4.4126	0.1971	-2.8592
2°ATD$_{Imm}$.491	-3.2439	-2.1680	1.6803
2°ATD$_{Imm}$.492	-2.4189	0.3303	3.3025
Variability	30.47%	19.05%	17.35%

Figure 13.
Principal component analysis of the 2° ATDImm LG.

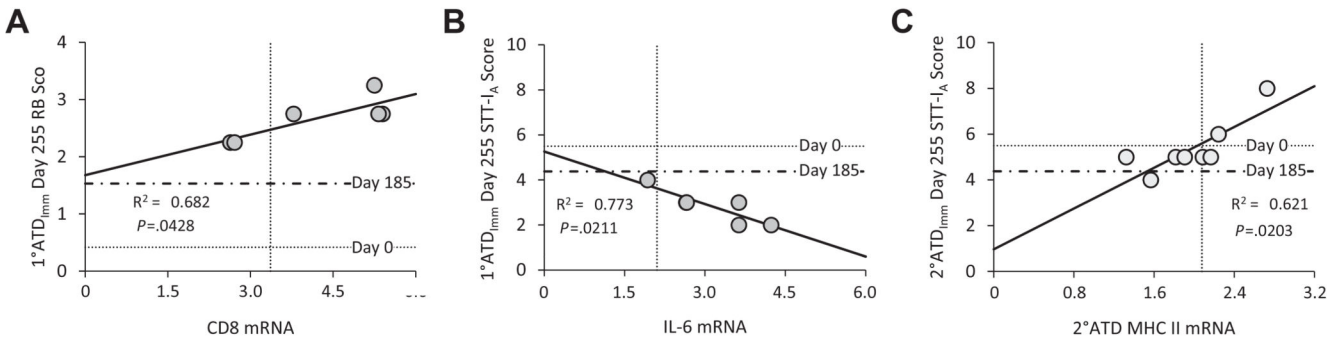

Figure 14.

Associations between ocular surface manifestations and transcript abundances. (A) 1° ATDImm eye day 255 rose Bengal staining score and 1° ATDImm LG CD8 mRNA abundance. (B) 1° ATDImm eye day 255 STT-IA score and 1° ATDImm LG IL 6 mRNA abundance. (C) 2° ATDImm eye day 255 STT-IA score and 2° ATDImm LG MHC II mRNA abundance.

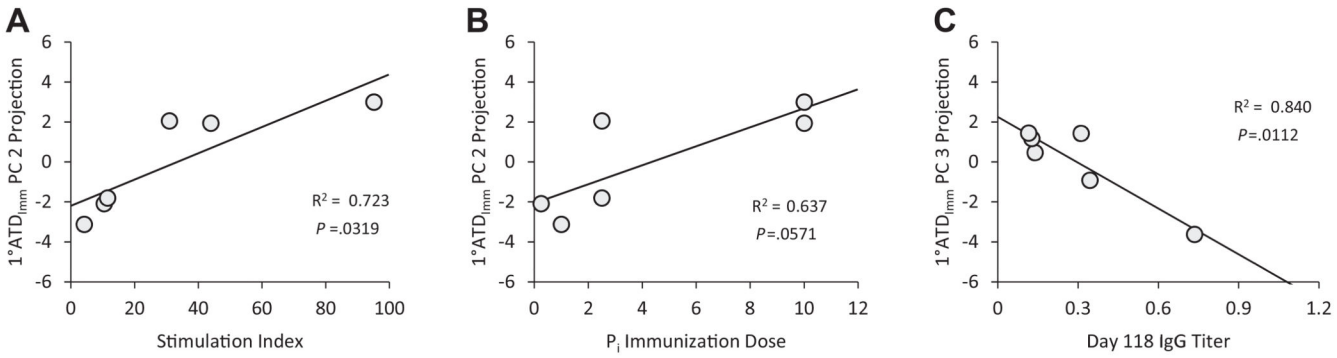

Figure 15.

Associations between 1° ATDImm LG PC 1, PC 2, and PC 3 projections and variables related to systemic immunization. (A) Relationship between 1° ATD(Imm)PC 2 projection and stimulation index. (B) Relationship between 1° ATD(Imm)PC 2 projection and initial immunizing Pi dose. (C) Relationship between 1° ATD(Imm)PC 3 projection and day 118 IgG titer.

Table 1

{PCI $^{\ominus}$} and {PCI $^{\oplus}$} comparisons

Variable	V82%, 29°		Control		1° ATD_{Imm}		2° ATD_{Imm}	
	{PC1 ⊖}	{PC1 ⊕}	{PC1 ⊖}	{PC1 ⊕}	{PC1 ⊖}	{PC1 ⊕}	{PC1 ⊖}	{PC1 ⊕}
IL-6	IL-6		IL-6			IL-6	IL-6	
IL-10	IL-10		IL-10		IL-10	←	→	IL-10
IL-17A	IL-17A		IL-17A		IL-17A	←	–	
BAFF	BAFF		BAFF			BAFF	–	
CD1d	CD1d		CD1d		CD1d	←	–	
CXCL13	CXCL13		CXCL13			CXCL13	CXCL13	
$RTLA^{+}$	$RTLA^{+}$		$RTLA^{+}$			$RTLA^{+}$	$RTLA^{+}$	
IL-1 β	IL-1 β		–			IL-1 β	IL-1b	
PRL	PRL		–		PRL	–	–	
CCL21	CCL21		–			CCL21	–	
CCL28	CCL28		–			–	–	CCL28
TNF-α		TNF-α	TNF-α			TNF-α		
MHC I		MHC I	MHC I			MHC I	MHC I	
CXCL8		CXCL8	CXCL8					
IL-12A		IL-12A	–		IL-12A			IL-12A
Perforin	N/A		Perforin		Perforin	←	→	Perforin
IL-18		IL-18		IL-18	→	IL-18	IL-18	
$CD18^{+}$				$CD18^{+}$	→	$CD18^{+}$	$CD18^{+}$	
MMP-9						MMP-9		MMP-9
IL-18R							IL-18R	

*Abundances of mRNAs for IL-2 and IL-4 were not included in PCA analyses of 1° ATDImm LG or 2° ATDImm LG because data were missing for one 1° ATDImm LG.